

Butterfly effect and $T\bar{T}$ -deformation

Debarshi Basu^{⊗,*†}, Ashish Chandra^{⊗,*‡} and Qiang Wen^{⊗§}

Shing-Tung Yau Center and School of Physics, Southeast University, Nanjing 210096, China

 (Received 22 July 2025; accepted 24 September 2025; published 12 November 2025)

These notes present a comprehensive analysis of shock wave geometries in holographic settings, focusing on $T\bar{T}$ -deformed Bañados–Teitelboim–Zanelli black holes and their extensions. By constructing deformed metrics and employing Kruskal coordinates, we examine out-of-time-ordered correlators as probes of quantum chaos. We also study localized shock wave solutions and analyze their backreaction, highlighting regimes in which the Mezei–Stanford bound on the butterfly velocity is potentially violated. The results obtained via shock wave methods are corroborated with recent developments in pole skipping phenomena and the entanglement wedge approach, demonstrating consistency among distinct probes of chaos in holographic theories.

DOI: [10.1103/qq7z-vkxv](https://doi.org/10.1103/qq7z-vkxv)

I. INTRODUCTION

The study of quantum chaos has emerged as a cornerstone of modern theoretical physics, offering profound insights into the dynamics of quantum systems, particularly those governed by strong interactions. In this context, black holes serve as natural objects for exploring quantum chaos, as their near-horizon geometries encode the scrambling of quantum information in dual field theories. Interestingly, various characteristic methods of chaos diagnostics have been proposed in the literature, such as out-of-time-ordered correlators (OTOCs), pole skipping, and the entanglement wedge method [1–5].

(i) The OTOCs shows an exponential behavior at late time caused due to small perturbations at early time. In particular, this is precisely captured by the growth of the four point correlator over time, resulting a characteristic exponential behavior described by the Lyapunov exponent. In chaotic systems, OTOCs typically exhibit exponential growth, approximated as

$$\langle V(t)W(0)V(t)W(0) \rangle \approx 1 - \epsilon e^{\lambda_L(t-t_*)}, \quad (1.1)$$

where λ_L is the Lyapunov exponent and t_* is described as the scrambling time, which indicates how

quickly information spreads across the quantum system [6,7].

In the context of AdS/CFT correspondence [8,9], eternal black holes are dual to thermofield double states of two coupled conformal field theories (CFTs) providing a natural framework to investigate quantum chaos. In this regard, the perturbations at early time applied on one side of the thermofield double state grow exponentially in time. In holographic settings, the OTOC takes the form¹

$$\mathcal{C}(t, x) \sim \exp \left[\lambda_L \left(t - t_* - \frac{|x|}{v_B} \right) \right], \quad (1.2)$$

where v_B and t_* are characteristic speed and time scales referred to as the butterfly velocity and the scrambling time. Here, the blueshift experienced by infalling quanta effectively converts a small initial perturbation into a shock wave in the bulk [3,7]. Furthermore, the authors of [33] also extended corresponding analysis for the dual OTOCs in localized shock wave configurations where it involves investigating a corresponding Ryu–Takayanagi (RT) surface discussed in [34–36]. Interestingly, the OTOCs in the bulk dual geometries depends on chaos parameters, such as the Lyapunov exponent and the butterfly velocity. In addition, it was proposed that these chaos parameters follow certain fundamental bounds. The Maldacena–Shenker–Stanford (MSS) bound limits the Lyapunov exponent to $\lambda_L \leq \frac{2\pi}{\beta}$, where β is the inverse temperature [37],

¹See also [10–32], for the further studies of OTOC and shock waves in various systems.

*These authors contributed equally to this work.

†Contact author: debarshi.128@gmail.com

‡Contact author: achandrahep@gmail.com

§Contact author: wenqiang@seu.edu.cn

Published by the American Physical Society under the terms of the [Creative Commons Attribution 4.0 International license](https://creativecommons.org/licenses/by/4.0/). Further distribution of this work must maintain attribution to the author(s) and the published article's title, journal citation, and DOI. Funded by SCOAP³.

while the Mezei-Stanford bound restricts the butterfly velocity to [5,38]

$$v_B \leq v_B^{\text{Sch}} = \sqrt{\frac{d}{2(d-1)}} \quad (1.3)$$

for theories dual to two-derivative gravity.

- (ii) The chaotic nature can also be captured by the properties of the retarded energy-density Green's function at the so called *pole skipping* points, which are holographically related to the near horizon properties of metric perturbations in the bulk [4,39–44]. Pole skipping occurs when lines of zeros and poles intersect. The frequency and momentum values where this happens are related to measures of chaos in the following way,

$$\omega_\star = i\lambda_L, \quad k_\star = i\frac{\lambda_L}{v_B}. \quad (1.4)$$

- (iii) The entanglement wedge method, on the other hand, offers a geometric perspective by analyzing the minimal boundary region containing a falling particle, providing a direct measure of v_B [5]. It links quantum states on the boundary to gravitational dynamics in the bulk, where a local perturbation, modeled as a particle falling toward a black hole horizon, causes information to delocalize over time.

On the other hand, the $\text{T}\bar{\text{T}}$ deformation introduces a novel, exactly solvable irrelevant double trace deformations in CFT_2 s that affects the ultraviolet behavior of the theories. This deformation is characterized by a term proportional to the determinant of the stress-energy tensor and governed by a parameter μ . It retains modular invariance [45–48], and also preserves the integrability of the original theory involving infinite set of conserved charges, which provides exact computations of critical quantities such as the energy spectrum, partition function, scattering S matrix, and entanglement and correlation properties [49–60]. In the literature, various holographic dual avatars for the $\text{T}\bar{\text{T}}$ deformed CFT_2 s have been proposed, including CFT coupled to topological gravity [46,61], noncritical string theory [62,63], AdS_3 (Anti-de Sitter) gravity at a finite radial cutoff [64–67],² the glue-on AdS holography [79,80], the mixed boundary conditions prescription in [81], as well as the dual gravity theory [82,83] of the random boundary geometry proposed in [45]. In this article, we will mostly focus on the mixed boundary conditions prescription, wherein the holographic dual of a $\text{T}\bar{\text{T}}$ deformed CFT_2 corresponds to AdS_3 gravity with mixed nonlinear boundary conditions at the asymptotic boundary [81], in contrast to the usual Dirichlet boundary conditions. This prescription is similar to the cutoff prescription in [64] in a sense that imposing Dirichlet boundary

conditions at a finite radial cutoff in the bulk is effectively equivalent to placing mixed boundary conditions at the asymptotics, on shell [84–86]. For a pedagogical review of the historical developments and more recent aspects of $\text{T}\bar{\text{T}}$ deformation and holography, the readers are directed to the reviews [87,88].

Interestingly, the nature of quantum chaos in the case of $\text{T}\bar{\text{T}}$ deformed theories was studied in earlier literature [52] where it was demonstrated that the OTOC in these field theories saturate the MSS bound and exhibit exponential structure at late times. In this work, we explore the impact of $\text{T}\bar{\text{T}}$ deformations on holographic quantum chaos. In the holographic context provided in [81], this deformation corresponds to a modified bulk geometry with the deformed field theory located at the asymptotic boundary. This geometric reinterpretation allows one to investigate the effects of $\text{T}\bar{\text{T}}$ deformations on the Bañados–Teitelboim–Zanelli (BTZ) black hole, dual to a deformed CFT_2 at finite temperature. In this regard, we obtain the OTOC through the computation of geodesic length in the nonrotating deformed BTZ black hole geometry in Kruskal coordinates. We follow corresponding analysis for both spherically symmetric and localized shock wave scenarios [7,33]. In this context, we observe a potential violation of the Mezei-Stanford bound [5] on the butterfly velocity. In undeformed holographic theories, this bound ensures that chaos spreads at a speed consistent with causality in the bulk. However, the $\text{T}\bar{\text{T}}$ deformation introduces nonlocal effects that may challenge these expectations, particularly for negative values of the deformation parameter. To probe this, we derive the butterfly velocity using three independent methods: the shock wave approach, pole skipping phenomena, and the entanglement wedge method. For rotating BTZ black holes, we extend our analysis to account for the conserved angular momentum. Here, we focus primarily on pole skipping and shock wave methods. The rotating case allows one to explore how the chemical potential for angular momentum modifies chaos parameters, particularly in near extremal limits where the inner and outer horizons coincide. We observe that the Lyapunov exponent consistently saturates the MSS bound across deformed and undeformed scenarios. In contrast, the butterfly velocity exhibits striking behavior: for negative deformation parameters, it can exceed the Mezei-Stanford bound, while near the Hagedorn bound it approaches zero.

In what follows, we outline the structure of our paper. In Sec. II, we present a detailed review of the construction of $\text{T}\bar{\text{T}}$ deformed BTZ black holes and the derivation of the deformed metric in Kruskal coordinates. Sec. III is devoted to the derivation of shock wave solutions in these deformed nonrotating BTZ geometries. We explicitly compute the blueshift factors and analyze OTOCs in the corresponding geometry. In Sec. IV, we carry out a detailed computation of OTOC in the deformed rotating BTZ background, extracting the modified Lyapunov exponent and butterfly velocity. Finally, in Sec. VI, we discuss our results for

²See also, [68–78] for further investigation in this direction.

holographic OTOCs, pole skipping, and the dynamics of quantum information scrambling. We conclude with a summary of our findings and a discussion of possible future directions.

II. A BRIEF REVIEW ON $T\bar{T}$ DEFORMATION AND HOLOGRAPHY

The $T\bar{T}$ deformation is a universal irrelevant deformation of a two-dimensional quantum field theory, generated by the determinant of the instantaneous stress tensor, and is governed by the flow equation [49,50,64,81],

$$\partial_\mu \mathcal{S}^{[\mu]} = -\frac{1}{2} \int d^2x \sqrt{\gamma^{[\mu]}} (\gamma_{ab} T^{ac} T^b{}_c - T^2)^{[\mu]}, \quad (2.1)$$

where the superscript $[\mu]$ denotes that the quantities correspond to the deformed theory and γ_{ab} describes the boundary metric. The stress tensor is, by definition, the response of $\mathcal{S}^{[\mu]}$ to arbitrary variations in the background metric,

$$\delta \mathcal{S}^{[\mu]} = \frac{1}{2} \int d^2x \sqrt{\gamma^{[\mu]}} T_{ab}^{[\mu]} \delta \gamma^{ab[\mu]}. \quad (2.2)$$

As described in [81], taking a variation of the defining relation (2.1) with respect to the background metric, one obtains after some simple algebra

$$\partial_\mu \gamma_{ab}^{[\mu]} = -2\hat{T}_{ab}^{[\mu]}, \quad \partial_\mu \hat{T}_{ab}^{[\mu]} = -\hat{T}_{ac}^{[\mu]} \hat{T}^{[b]c}_{\mu}, \quad (2.3)$$

where $\hat{T}_{ab} = T_{ab} - \gamma_{ab} T$ is the trace reversed stress tensor. These equations are easily solved in terms of the undeformed metric and stress tensors $(\gamma_{ab}^{[0]}, \hat{T}_{ab}^{[0]})$ as follows [81]

$$\begin{aligned} \gamma_{ab}^{[\mu]} &= \gamma_{ab}^{[0]} - 2\mu \hat{T}_{ab}^{[0]} + \mu^2 \hat{T}_{ac}^{[0]} \hat{T}_{db}^{[0]} \gamma^{[0]cd}, \\ \hat{T}_{ab}^{[\mu]} &= \hat{T}_{ab}^{[0]} - \mu \hat{T}_{ac}^{[0]} \hat{T}_{db}^{[0]} \gamma^{[0]cd}. \end{aligned} \quad (2.4)$$

Note that the above solutions are exact in the deformation parameter, and not perturbative.

Holography: In order to obtain the deformed dictionary, we begin with the Fefferman-Graham radial gauge ($g_{\rho a} = 0$)

$$ds^2 = \ell^2 \frac{d\rho^2}{4\rho^2} + g_{ab} dx^a dx^b, \quad g_{ab} = \frac{1}{\rho} g_{ab}^{(0)} + g_{ab}^{(2)} + \rho g_{ab}^{(4)}. \quad (2.5)$$

In the case of pure gravity, the undeformed dictionary is given as follows [89]

$$\gamma_{ab}^{[0]} = g_{ab}^{(0)}, \quad g_{ab}^{(2)} = 8\pi G_N \ell^2 \hat{T}_{ab}^{[0]}, \quad g_{ab}^{(4)} = \frac{1}{4} g_{ab}^{(2)} g^{(0)cd} g_{db}^{(0)}. \quad (2.6)$$

One may now easily find the following nonlinear and rather mixed boundary conditions (involving both $g^{(0)}$ and $g^{(2)}$ as compared to only $g^{(0)}$ in the case with Dirichlet boundary conditions) for the $T\bar{T}$ -deformed theory

$$\gamma_{ab}^{[\mu]} = g_{ab}^{(0)} - \frac{\mu}{4\pi G_N \ell} g_{ab}^{(2)} + \left(\frac{\mu}{4\pi G_N \ell} \right)^2 g_{ab}^{(4)} \equiv \rho_c g_{ab}(\rho_c), \quad (2.7)$$

where $\rho_c = -\frac{\mu}{4\pi G_N \ell}$ and hence $\gamma_{ab}^{[\mu]}$ may be identified as the induced metric on the $\rho = \rho_c$ slice, in accordance with the cutoff prescription in [64].

A. The deformed spacetime: Flat background

Finding the most general solution for the bulk metric compatible with the holographic Ward identities [89] as well as the nonlinear mixed boundary conditions in Eqs. (2.4) and (2.7) is, in general, a complicated issue. However, for a deformed theory on flat background, it is particularly simple as $g^{(0)}$ and $\gamma^{[\mu]}$ are diffeomorphic to one another [81]. In this case, the most general deformed bulk metric may be obtained by applying a two-dimensional coordinate transformation to the generic bulk metric with a flat background ($g^{(0)} = \eta$), namely the Banados metric [90]

$$\begin{aligned} ds^2 &= \ell^2 \frac{d\rho^2}{4\rho^2} + \frac{dwd\bar{w}}{\rho} + \mathcal{L}_\mu(w) dw^2 + \bar{\mathcal{L}}_\mu(\bar{w}) d\bar{w}^2 \\ &\quad + \rho \mathcal{L}_\mu(w) \bar{\mathcal{L}}_\mu(\bar{w}) dw d\bar{w}, \end{aligned} \quad (2.8)$$

where (w, \bar{w}) denotes the boundary coordinates of the auxiliary flat background discussed above. Therefore, the deformed dictionary (2.7) yields

$$\begin{aligned} \gamma_{ab}^{[\mu]} dx^a dx^b &= (dw + \rho_c \bar{\mathcal{L}}_\mu(\bar{w}) d\bar{w})(d\bar{w} + \rho_c \mathcal{L}_\mu(w) dw) \\ &\equiv dZ d\bar{Z}, \end{aligned} \quad (2.9)$$

where, (Z, \bar{Z}) are the coordinates that describe the deformed CFT. The two sets of coordinates are related through the following state-dependent coordinate transformations³

$$Z = w + \rho_c \int^{\bar{w}} \bar{\mathcal{L}}_\mu(\bar{w}) d\bar{w}, \quad \bar{Z} = \bar{w} + \rho_c \int^w \mathcal{L}_\mu(w) dw. \quad (2.10)$$

³The functions $\mathcal{L}_\mu, \bar{\mathcal{L}}_\mu$ are related to the stress tensor expectation values on the auxiliary flat boundary, which renders the coordinate transformation (2.10) dynamical. See, for example, [45].

The Fefferman-Graham expansion of the deformed metric may then be obtained by acting on with the inverse coordinate transformations

$$\begin{pmatrix} dw \\ d\bar{w} \end{pmatrix} = \frac{1}{1 - \rho_c^2 \mathcal{L}_\mu(w) \bar{\mathcal{L}}_\mu(\bar{w})} \begin{pmatrix} 1 & -\rho_c \bar{\mathcal{L}}_\mu(\bar{w}) \\ -\rho_c \mathcal{L}_\mu(w) & 1 \end{pmatrix} \times \begin{pmatrix} dZ \\ d\bar{Z} \end{pmatrix}, \quad (2.11)$$

on each of the metric coefficients of the auxiliary Banados geometry (2.8).

III. DEFORMED BTZ BLACK HOLE

A typical example of the deformed spacetime is given by the nonrotating BTZ black hole dual to a $\text{T}\bar{\text{T}}$ -deformed CFT_2 at finite temperature, for which $\mathcal{L}_\mu = \bar{\mathcal{L}}_\mu = \text{const.}$ Utilizing the inverse transformations (2.11) and subsequently making the coordinate transformations [81,91]

$$r = \frac{1 + \mathcal{L}_\mu \rho}{\sqrt{\rho}}, \quad Z = x + t, \quad \bar{Z} = x - t, \quad (3.1)$$

one obtains⁴

$$\begin{aligned} ds^2 = & -(r^2 - 4\mathcal{L}_\mu) \frac{dt^2}{(1 + 2\mu\mathcal{L}_\mu)^2} + \frac{dr^2}{r^2 - 4\mathcal{L}_\mu} \\ & + r^2 \frac{dx^2}{(1 - 2\mu\mathcal{L}_\mu)^2} \\ x \sim & x + 2\pi. \end{aligned} \quad (3.2)$$

The event horizon is located at $r = 2\sqrt{\mathcal{L}_\mu}$ and the inverse temperature is given by

$$\beta = \frac{\pi}{\sqrt{\mathcal{L}_\mu}} (1 + 2\mu\mathcal{L}_\mu). \quad (3.3)$$

Note that β has to be identified with the temperature of the deformed CFT_2 and hence the parameter \mathcal{L}_μ should be understood as a function of μ according to the above expression.

Kruskal extension: Under the coordinate transformations

$$r = 2\sqrt{\mathcal{L}_\mu} \frac{1 - uv}{1 + uv}, \quad t = \frac{1 + 2\mu\mathcal{L}_\mu}{4\sqrt{\mathcal{L}_\mu}} \log\left(-\frac{v}{u}\right), \quad (3.4)$$

the deformed BTZ black hole metric may be rewritten in the Kruskal form

⁴In this article, we set AdS length scale to unity $\ell = 1$ and rescale the deformation parameter as $\mu \rightarrow \frac{\mu}{8\pi G_N}$.

$$ds^2 = -\frac{4dudv}{(1 + uv)^2} + 4\mathcal{L}_\mu \left(\frac{1 - uv}{1 + uv}\right)^2 \frac{dx^2}{(1 - 2\mu\mathcal{L}_\mu)^2}. \quad (3.5)$$

Note that the Kruskal coordinates (u, v, x) smoothly cover the maximally extended black hole spacetime, dual to the thermofield double state in the deformed CFT_2 [92]. The boundaries are at $uv = -1$, while the event horizons and the future and past singularities are given, respectively, by $uv = 0$ and $uv = 1$. The inverse coordinate transformations may also be obtained for the left and right geometries, respectively, as follows

$$\begin{aligned} \text{(left)} \quad u &= e^{-\frac{2\sqrt{\mathcal{L}_\mu}}{1+2\mu\mathcal{L}_\mu}t} \sqrt{\frac{r - 2\sqrt{\mathcal{L}_\mu}}{r + 2\sqrt{\mathcal{L}_\mu}}}, \\ v &= -e^{\frac{2\sqrt{\mathcal{L}_\mu}}{1+2\mu\mathcal{L}_\mu}t} \sqrt{\frac{r - 2\sqrt{\mathcal{L}_\mu}}{r + 2\sqrt{\mathcal{L}_\mu}}}, \\ \text{(right)} \quad u &= -e^{-\frac{2\sqrt{\mathcal{L}_\mu}}{1+2\mu\mathcal{L}_\mu}t} \sqrt{\frac{r - 2\sqrt{\mathcal{L}_\mu}}{r + 2\sqrt{\mathcal{L}_\mu}}}, \\ v &= e^{\frac{2\sqrt{\mathcal{L}_\mu}}{1+2\mu\mathcal{L}_\mu}t} \sqrt{\frac{r - 2\sqrt{\mathcal{L}_\mu}}{r + 2\sqrt{\mathcal{L}_\mu}}}. \end{aligned} \quad (3.6)$$

Embedding in $\mathbb{R}^{2,2}$: The deformed geometry is still asymptotically AdS_3 (maximally symmetric) and therefore can be embedded in $\mathbb{R}^{2,2}$ with a quadratic constraint as follows

$$ds^2 = \eta_{AB} dX^A dX^B, \quad X^2 \equiv \eta_{AB} X^A X^B = -1, \quad (3.7)$$

where the standard metric on $\mathbb{R}^{2,2}$ is given by $\eta = \text{diag}(-1, -1, 1, 1)$. For example, an embedding ansatz is given by [7],

$$\begin{aligned} X_1 &= \frac{v + u}{1 + uv} = \sqrt{\frac{r^2}{4\mathcal{L}_\mu} - 1} \sinh\left(\frac{2\sqrt{\mathcal{L}_\mu}t}{1 + 2\mu\mathcal{L}_\mu}\right), \\ X_2 &= \frac{1 - uv}{1 + uv} \cosh\left(\frac{2\sqrt{\mathcal{L}_\mu}x}{1 - 2\mu\mathcal{L}_\mu}\right) = \frac{r}{2\sqrt{\mathcal{L}_\mu}} \cosh\left(\frac{2\sqrt{\mathcal{L}_\mu}x}{1 - 2\mu\mathcal{L}_\mu}\right), \\ X_3 &= \frac{v - u}{1 + uv} = \sqrt{\frac{r^2}{4\mathcal{L}_\mu} - 1} \cosh\left(\frac{2\sqrt{\mathcal{L}_\mu}t}{1 + 2\mu\mathcal{L}_\mu}\right), \\ X_4 &= \frac{1 - uv}{1 + uv} \sinh\left(\frac{2\sqrt{\mathcal{L}_\mu}x}{1 - 2\mu\mathcal{L}_\mu}\right) = \frac{r}{2\sqrt{\mathcal{L}_\mu}} \sinh\left(\frac{2\sqrt{\mathcal{L}_\mu}x}{1 - 2\mu\mathcal{L}_\mu}\right). \end{aligned} \quad (3.8)$$

The geodesic length between two arbitrary bulk points $X^A \equiv (u, v, x)$ and $X^A \equiv (u', v', x')$ may be computed in the embedding coordinates, as

$$\begin{aligned}
 d(X, X') &= \text{arccosh}(-X \cdot X') \\
 &= \text{arccosh} \left[\frac{2(uv' + vu') + (1 - uv)(1 - u'v') \cosh \left[\frac{2\sqrt{\mathcal{L}_\mu}(x-x')}{1-2\mu\mathcal{L}_\mu} \right]}{(1 + uv)(1 + u'v')} \right], \quad (3.9)
 \end{aligned}$$

where the dot product is taken with respect to the metric η_{AB} .

A. Spherically symmetric shock wave

In this subsection, following [7], we perturb the dual thermofield double state (TFD) by adding a few quantas at the left boundary and analyze the effects of the gravitational shock wave in the deformed bulk geometry. Our goal is to study the OTOC in the TFD state,

$$\langle W(t_2, x_2)V(t_1, x_1)W(t_2, x_2)V(t_1, x_1) \rangle_\beta, \quad (3.10)$$

where $t_2 - t_1 \gg \beta$. In the Kruskal coordinates, the OTOC may be interpreted as a gravitational scattering problem between the W and V particles, whose dual operators are inserted in the boundary state [3,7].

Now, we mildly perturb the deformed black hole spacetime by adding a few particles at the left boundary, and let them fall into the black hole as depicted in Fig. 1. As customary, we shall designate these particles by W . Although the particles have a very small energy that does not seem to perturb the background geometry significantly, one should note the following:

Fact: If a particle released from the boundary $r \rightarrow \infty$ at an early time t_W is moving along a null trajectory with proper energy E , then the energy E_r measured on the time slice $t = 0$ is given by

$$E_r = \frac{E}{\sqrt{g_{00}|_{t=0}}}. \quad (3.11)$$

For the deformed BTZ black hole (3.2), the null trajectories may be found by defining the tortoise coordinate⁵ as follows

$$\begin{aligned}
 dr_\star &= (1 + 2\mu\mathcal{L}_\mu) \frac{dr}{r^2 - 4\mathcal{L}_\mu} \Rightarrow r_\star \\
 &= \frac{(1 + 2\mu\mathcal{L}_\mu)}{4\sqrt{\mathcal{L}_\mu}} \log \left(\frac{r - 2\sqrt{\mathcal{L}_\mu}}{r + 2\sqrt{\mathcal{L}_\mu}} \right). \quad (3.13)
 \end{aligned}$$

Therefore, the null trajectories are given by

⁵In terms of the tortoise coordinate, the Kruskal coordinates may be rewritten in the familiar form,

$$u = -e^{-\frac{2\sqrt{\mathcal{L}_\mu}}{1+2\mu\mathcal{L}_\mu}(t-r_\star)}, \quad v = e^{\frac{2\sqrt{\mathcal{L}_\mu}}{1+2\mu\mathcal{L}_\mu}(t+r_\star)}. \quad (3.12)$$

$$\begin{aligned}
 -(r^2 - 4\mathcal{L}_\mu) \frac{dt^2}{(1 + 2\mu\mathcal{L}_\mu)^2} + \frac{dr^2}{r^2 - 4\mathcal{L}_\mu} &= 0, \\
 \Rightarrow \int_{t_W}^t dt &= \int_0^{r_\star} dr_\star \Rightarrow t = t_W + r_\star. \quad (3.14)
 \end{aligned}$$

Hence, the blue-shifted energy at the time slice $t = 0$ is given by

$$E_r = \frac{1 + 2\mu\mathcal{L}_\mu}{\sqrt{r^2 - 4\mathcal{L}_\mu}|_{t=0}} E \sim \frac{E(1 + 2\mu\mathcal{L}_\mu)}{2\sqrt{\mathcal{L}_\mu}} e^{\frac{2\sqrt{\mathcal{L}_\mu}}{1+2\mu\mathcal{L}_\mu}t_W}. \quad (3.15)$$

From the above expression it is clear that, if t_W is sufficiently large, we must include the effects of back-reaction of this energy. Similar to the undeformed case described in [7], we construct the geometry by gluing a deformed BTZ metric of mass M to that of mass $M + E$ across the null surface

$$u_W = e^{-\frac{2\sqrt{\mathcal{L}_\mu}}{1+2\mu\mathcal{L}_\mu}t_W}, \quad (3.16)$$

where $E \ll M$ is the asymptotic energy of the perturbation. We will use coordinates (u, v) to the right of the shell and (\hat{u}, \hat{v}) to the left as depicted in Fig. 1. It is straightforward to verify that the horizon radii scales as

$$\hat{\mathcal{L}}_\mu = \frac{E + M}{M} \mathcal{L}_\mu. \quad (3.17)$$

Similar to the undeformed case [7], we will use the matching conditions

- (1) The time coordinate t flows continuously across the shell.

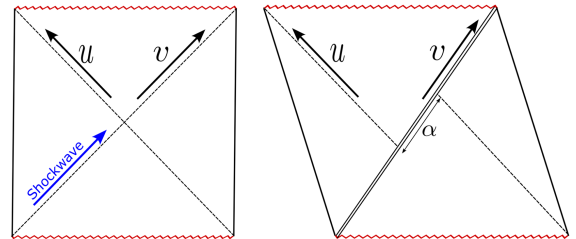


FIG. 1. (Left panel) Insertion of a few particles from the left boundary leads to a gravitational shock wave in the bulk geometry. (Right panel) The Penrose diagram after the shock wave insertion, depicted by the double line. The dashed $v = 0$ and $\bar{v} = 0$ horizons miss by an amount α .

(2) The radius of the S^1 is continuous across the shell. The first condition determines the location of the shell in terms of the hatted coordinates as

$$\hat{u}_W = e^{\frac{2\sqrt{\hat{\mathcal{L}}}_\mu}{1+2\mu\hat{\mathcal{L}}_\mu} t_W}, \quad (3.18)$$

whereas the second condition implies the following relation

$$\frac{\sqrt{\hat{\mathcal{L}}}_\mu}{1-2\mu\hat{\mathcal{L}}_\mu} \frac{1-\hat{u}_W\hat{v}}{1+\hat{u}_W\hat{v}} = \frac{\sqrt{\mathcal{L}}_\mu}{1-2\mu\mathcal{L}_\mu} \frac{1-u_Wv}{1+u_Wv}. \quad (3.19)$$

For small $\frac{E}{M}$, the above relation may be solved straightforwardly to obtain

$$\hat{v} = v + \alpha, \quad \alpha = \frac{E}{4M} \frac{1+2\mu\mathcal{L}_\mu}{1-2\mu\mathcal{L}_\mu} e^{\frac{2\sqrt{\mathcal{L}}_\mu}{1+2\mu\mathcal{L}_\mu} t_W}. \quad (3.20)$$

This matching condition is exact in the limit $\frac{E}{M} \rightarrow 0$ and $t_W \rightarrow \infty$ with α fixed. Furthermore, in this limit, we have $\hat{\mathcal{L}}_\mu = \mathcal{L}_\mu$ and hence the bulk metric may be written as

$$ds^2 = \frac{-4dudv}{[1+u(v+\alpha\Theta(u))]^2} + 4\mathcal{L}_\mu \left[\frac{1-u(v+\alpha\Theta(u))}{1+u(v+\alpha\Theta(u))} \right]^2 \times \frac{dx^2}{(1-2\mu\mathcal{L}_\mu)^2}. \quad (3.21)$$

In terms of the discontinuous coordinates $\bar{u} = u$, $\bar{v} = v + \alpha\Theta(u)$, the metric takes a more standard shock wave form

$$ds^2 = \frac{-4d\bar{u}d\bar{v} + 4\alpha\delta(\bar{u})d\bar{u}^2}{(1+\bar{u}\bar{v})^2} + 4\mathcal{L}_\mu \left(\frac{1-\bar{u}\bar{v}}{1+\bar{u}\bar{v}} \right)^2 \frac{dx^2}{(1-2\mu\mathcal{L}_\mu)^2}. \quad (3.22)$$

It is straightforward to check that Einstein equations imply a stress tensor

$$d_1 = \text{arccosh} \left[\frac{r}{2\sqrt{\mathcal{L}}_\mu} \cosh \frac{2\sqrt{\mathcal{L}}_\mu(x-x_0)}{1-2\mu\mathcal{L}_\mu} + \frac{\sqrt{r^2-4\mathcal{L}_\mu}}{2\sqrt{\mathcal{L}}_\mu} (v+\alpha) e^{\frac{2\sqrt{\mathcal{L}}_\mu t_L}{1+2\mu\mathcal{L}_\mu}} \right], \quad (3.24)$$

where we have used the fact that, on the left geometry

$$u_L = \frac{\sqrt{r^2-4\mathcal{L}_\mu}}{r+2\sqrt{\mathcal{L}}_\mu} e^{\frac{2\sqrt{\mathcal{L}}_\mu t_L}{1+2\mu\mathcal{L}_\mu}}, \quad v_L = -\frac{\sqrt{r^2-4\mathcal{L}_\mu}}{r+2\sqrt{\mathcal{L}}_\mu} e^{\frac{2\sqrt{\mathcal{L}}_\mu t_L}{1+2\mu\mathcal{L}_\mu}}.$$

In a similar manner,

$$d_2 = \text{arccosh} \left[\frac{r}{2\sqrt{\mathcal{L}}_\mu} \cosh \frac{2\sqrt{\mathcal{L}}_\mu(x-x_0)}{1-2\mu\mathcal{L}_\mu} - \frac{\sqrt{r^2-4\mathcal{L}_\mu}}{2\sqrt{\mathcal{L}}_\mu} v e^{\frac{2\sqrt{\mathcal{L}}_\mu t_R}{1+2\mu\mathcal{L}_\mu}} \right]. \quad (3.25)$$

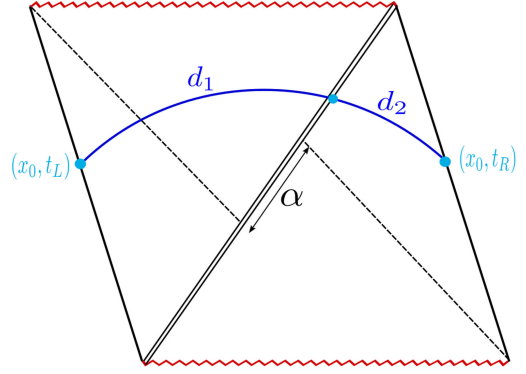


FIG. 2. Computing the geodesic distance between two points (x_0, t_L) and (x_0, t_R) on the left and right asymptotic boundaries in the shock wave geometry.

$$T_{uu} = \frac{\alpha}{4\pi G_N} \delta(u), \quad (3.23)$$

corresponding to a shell of null particles symmetrically distributed on the horizon.

1. Geodesics and shock wave effects: OTOC

Consider a geodesic connecting a point at Killing time t_L on the left boundary with a point at Killing time t_R on the right boundary. We will take both points to be located at the same value of $x = x_0$. As depicted in Fig. 2, such a geodesic is made up of two geodesic segments on the left and right of the shock wave, respectively, which are joined smoothly at the horizon $u = 0$. In Fig. 2, d_1 corresponds to the length between the boundary point $(u_\infty^L, v_\infty^L, x_0)$ (the subscript ∞ is used to denote the boundary point) and an arbitrary point $(0, v + \alpha, x)$ on the horizon. Similarly, d_2 denotes the geodesic length between $(0, v, x)$ and $(u_\infty^R, v_\infty^R, x_0)$ on the right Kruskal geometry. Using the geodesic distance formula (3.9) in embedding coordinates, we may now obtain

For large $r = r_\infty$, from Eq. (3.6) we may obtain the total length of the two segments as

$$d = \log \left[\frac{r_\infty^2}{\mathcal{L}_\mu} \left(\cosh \frac{2\sqrt{\mathcal{L}_\mu}(x-x_0)}{1-2\mu\mathcal{L}_\mu} + (v+\alpha)e^{-\frac{2\sqrt{\mathcal{L}_\mu}t_L}{1+2\mu\mathcal{L}_\mu}} \right) \left(\cosh \frac{2\sqrt{\mathcal{L}_\mu}(x-x_0)}{1-2\mu\mathcal{L}_\mu} - ve^{-\frac{2\sqrt{\mathcal{L}_\mu}t_R}{1+2\mu\mathcal{L}_\mu}} \right) \right]. \quad (3.26)$$

Now extremizing the total length over the arbitrary parameters (x, v) , we obtain

$$x = x_0, \quad v = \frac{1}{2} \left(-e^{-\frac{2\sqrt{\mathcal{L}_\mu}t_L}{1+2\mu\mathcal{L}_\mu}} + e^{\frac{2\sqrt{\mathcal{L}_\mu}t_R}{1+2\mu\mathcal{L}_\mu}} - \alpha \right), \quad (3.27)$$

leading to the minimal geodesic distance

$$\begin{aligned} d_{\min} &= 2 \log \left[\frac{r_\infty}{\sqrt{\mathcal{L}_\mu}} \left(\cosh \frac{\sqrt{\mathcal{L}_\mu}(t_L-t_R)}{1+2\mu\mathcal{L}_\mu} + \frac{\alpha}{2} e^{-\frac{\sqrt{\mathcal{L}_\mu}}{1+2\mu\mathcal{L}_\mu}(t_L+t_R)} \right) \right] \\ &= 2 \log \left[\frac{\beta + \sqrt{\beta^2 - 8\pi^2\mu}}{2\pi\epsilon_c} \left(\cosh \frac{\pi(t_L-t_R)}{\beta} + \frac{\alpha}{2} e^{-\frac{\pi(t_L+t_R)}{\beta}} \right) \right], \end{aligned} \quad (3.28)$$

where we have used the cutoff $\epsilon_c = 1/r_\infty$ for large r . The first term in the parenthesis is the usual Hartman-Maldacena contribution [93], whereas the second term proportional to α corresponds to the effect of the shock wave. Note that for large t_L, t_R the effect of the shock wave on the geodesic distance becomes negligible as in the undeformed case.

2. OTOC

In the geodesic approximation, the OTOC may be obtained as the two point function of the (quasiprimary) fields V_L and V_R in the left and right CFTs respectively, computed in the perturbed geometry where a W operator creates a few particles at far past t_W . Assuming that the saddle point approximation still holds for the gravitational path integral, we may obtain this correlation function in the geodesic approximation in terms of a particle of mass m following a geodesic trajectory in the bulk [7],

$$\begin{aligned} &\langle W(t_W)V_L(0)V_R(0)W(t_W) \rangle \\ &\equiv \langle W(t_W)|V_L V_R|W(t_W) \rangle \approx e^{-m_W d}. \end{aligned} \quad (3.29)$$

For $t_L = t_R = 0$, we have the following estimate for the OTOC:

$$\frac{\langle V_L V_R \rangle_W}{\langle W W \rangle \langle V_L V_R \rangle} \sim \left[\frac{1}{1 + \frac{E}{8M} \frac{1+2\mu\mathcal{L}_\mu}{1-2\mu\mathcal{L}_\mu} e^{\frac{2\sqrt{\mathcal{L}_\mu}}{1+2\mu\mathcal{L}_\mu} t_W}} \right]^{2m_W}, \quad (3.30)$$

which enables us to identify the Lyapunov exponent as [cf. Eq. (3.3)]

$$\lambda_L = \frac{2\sqrt{\mathcal{L}_\mu}}{1+2\mu\mathcal{L}_\mu} = \frac{2\pi}{\beta}. \quad (3.31)$$

Therefore, we may conclude that the MSS bound [37] is saturated even for the deformed CFT₂.

B. Localized shock

For a more realistic scenario, in this section, we consider a localized shock wave introduced in [94,95].⁶ In particular, the authors of [94] considered spherical shock wave generated by a massless particle, moving along the horizon of a Schwarzschild black hole. This shock wave is localized on the null hypersurface at the horizon ($u = 0$), causing a coordinate shift in the null coordinate v . The metric of a generic two-sided static black hole in null coordinates is given by,

$$ds^2 = 2A(u, v)du dv + B(u, v)dx^2. \quad (3.32)$$

In the present scenario, from Eq. (3.5), we may identify

$$A(u, v) = \frac{-2}{(1+uv)^2}, \quad B(u, v) = \frac{4\mathcal{L}_\mu}{(1-2\mu\mathcal{L}_\mu)^2} \left(\frac{1-uv}{1+uv} \right)^2. \quad (3.33)$$

The (unperturbed) background obeys the Einstein equations

$$R_{\mu\nu} - \frac{1}{2}g_{\mu\nu}R + \Lambda g_{\mu\nu} = \kappa_G T_{\mu\nu}, \quad \kappa_G = 8\pi G_N, \quad (3.34)$$

where the matter stress tensor may be obtained as follows

$$T_{\mu\nu}^{\text{matter}} dx^\mu dx^\nu = T_{uu} du^2 + 2T_{uv} du dv + T_{vv} dv^2 + T_{xx} dx^2. \quad (3.35)$$

⁶For further studies in similar geometries, see also [96–99].

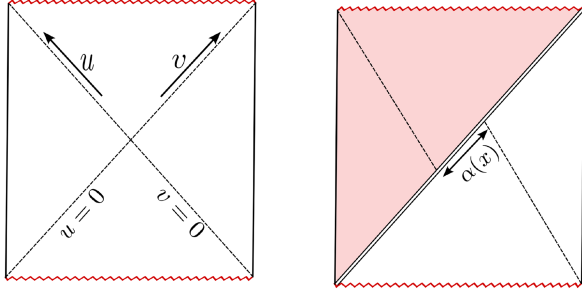


FIG. 3. Localized shock.

The components of the matter stress tensor may be obtained from the Einstein equations, in terms of the functions A , B as follows

$$\begin{aligned}\kappa_G T_{uu} &= \frac{A(\partial_u B)^2 + 2B(\partial_u A \partial_u B - A \partial_u^2 B)}{4AB^2}, \\ \kappa_G T_{vv} &= \frac{A(\partial_v B)^2 + 2B(\partial_v A \partial_v B - A \partial_v^2 B)}{4AB^2}, \\ \kappa_G T_{uv} &= \frac{2B \partial_u \partial_v B - \partial_u B \partial_v B}{4B^2} - A, \\ \kappa_G T_{xx} &= \frac{B}{A^3} (A \partial_u \partial_v A - \partial_u A \partial_v A - A^3). \end{aligned} \quad (3.36)$$

In the following, we will investigate the effects of inserting a shock wave in the background (3.32) and subsequently compute the OTOC in geodesic approximation.

1. Backreaction due to shock wave

We consider the shock wave with stress-energy tensor

$$T_{uu}^{\text{shock}} = E_0 e^{\frac{2u}{\beta}} \delta(u) \delta(x), \quad (3.37)$$

localized on the horizon $u = 0$ at $x = 0$. Here, E_0 is a constant related to the asymptotic energy of the shock wave and $e^{\frac{2u}{\beta}}$ represents the blue-shift factor. Upon introduction of the shock, the metric in the red region in Fig. 3 will change. The shock wave geometry is characterized by the shift [94,95,97]

$$\begin{aligned} u &\rightarrow u, & v &\rightarrow v + \Theta(u) \alpha(t, x), \\ du &\rightarrow du, & dv &\rightarrow dv + \alpha(t, x) \delta(u) du. \end{aligned} \quad (3.38)$$

As earlier, we may redefine the Kruskal coordinates as [7,33]

$$\bar{u} = u, \quad \bar{v} = v + \Theta(u) \alpha(t, x), \quad \bar{x} = x. \quad (3.39)$$

In terms of the new coordinates, the shock wave metric looks like

$$ds^2 = 2A(\bar{u}, \bar{v}) d\bar{u} d\bar{v} + B(\bar{u}, \bar{v}) d\bar{x}^2 - 2A(\bar{u}, \bar{v}) \alpha(\bar{x}) \delta(\bar{u}) d\bar{u}^2. \quad (3.40)$$

The backreacted Einstein equations take the form

$$R_{\mu\nu} - \frac{1}{2} g_{\mu\nu} R + \Lambda g_{\mu\nu} = \kappa (T_{\mu\nu}^{\text{matter}} + T_{\mu\nu}^{\text{shock}}), \quad (3.41)$$

where the matter part takes the following form in the barred coordinates [cf. Eq. (3.35)]

$$\begin{aligned} T_{\mu\nu}^{\text{matter}} dx^\mu dx^\nu &= (T_{\bar{u}\bar{u}} + \alpha(t, x)^2 \delta(u)^2 T_{\bar{v}\bar{v}} \\ &\quad - 2\alpha(t, x) \delta(u) T_{\bar{u}\bar{v}}) d\bar{u}^2 \\ &\quad + 2(T_{\bar{u}\bar{v}} - 2\alpha(t, x) \delta(u) T_{\bar{v}\bar{v}}) d\bar{u} d\bar{v} \\ &\quad + T_{\bar{v}\bar{v}} d\bar{v}^2 + T_{\bar{x}\bar{x}} d\bar{x}^2. \end{aligned} \quad (3.42)$$

To keep track of the order of perturbation we multiply the source and the effect of geometric shift with a constant book keeping parameter σ ,

$$T_{\mu\nu}^{\text{shock}} \rightarrow \sigma T_{\mu\nu}^{\text{shock}}, \quad \alpha \rightarrow \sigma \alpha.$$

Then the $\bar{v}\bar{v}$ component of the Einstein equations at the linear order in σ gives the following differential equation

$$\begin{aligned} \left(\partial_x^2 - \frac{\partial_u \partial_v B}{2A} \right) \alpha(x) &= 8\pi G_N \frac{B}{A} E_0 e^{\frac{2u}{\beta}} \delta(x), \\ \text{or, } (\partial_x^2 - \mathcal{M}(u, v)^2) \alpha(x) &= -e^{\frac{2u}{\beta}(t-t_*)} \delta(x), \end{aligned} \quad (3.43)$$

where, we have defined

$$\mathcal{M}(u, v) = \sqrt{\frac{\partial_u \partial_v B}{2A}}, \quad t_* = \frac{\beta}{2\pi} \log \left(\frac{A}{8\pi G_N E_0 B} \right). \quad (3.44)$$

Our job is to solve the above equation near the horizon $u = 0$, whence, using Eq. (3.33),

$$\begin{aligned} \mathcal{M}^2 &= \frac{\partial_u \partial_v B}{2A} \Big|_{u=0} = \frac{4\pi^2}{\beta^2 - 8\pi^2 \mu}, \\ t_* &= \frac{\beta}{2\pi} \log \left(\frac{\beta^2 - 8\pi^2 \mu}{16\pi^3 G_N E_0} \right). \end{aligned} \quad (3.45)$$

The homogeneous equation has the following solution:

$$\alpha(x) = \begin{cases} c_1 e^{\mathcal{M}x} + c_2 e^{-\mathcal{M}x} & \text{for } x < 0, \\ c_3 e^{\mathcal{M}x} + c_4 e^{-\mathcal{M}x} & \text{for } x > 0. \end{cases}$$

The delta function contributes to the first order discontinuity,

$$\alpha'(\epsilon) - \alpha'(-\epsilon) = -e^{\frac{2\pi}{\beta}(t-t_*)}, \quad (3.46)$$

where $\epsilon \rightarrow 0$ is a small parameter. These conditions lead to

$$c_1 - c_3 = c_4 - c_2 = \frac{1}{2\mathcal{M}} e^{\frac{2\pi}{\beta}(t-t_*)}. \quad (3.47)$$

We may choose $c_2 = c_3 = 0$ [100], to obtain the final profile of the shock wave as

$$\alpha(x) = \frac{1}{2\mathcal{M}} e^{\frac{2\pi}{\beta}(t-t_* - \frac{\beta\mathcal{M}}{2\pi}x)}. \quad (3.48)$$

Upon determining the shock wave profile, a straightforward analysis of a geodesic connecting two points on the left and right asymptotic boundaries of the shock wave geometry will lead to the OTOC,

$$\frac{\langle V_L V_R \rangle_W}{\langle WW \rangle \langle V_L V_R \rangle} \sim \left[\frac{1}{1 + \frac{1}{4\mathcal{M}} e^{\frac{2\pi}{\beta}(t-t_* - \frac{\beta\mathcal{M}}{2\pi}x)}} \right]^{2m_W}, \quad (3.49)$$

Therefore, the Lyapunov exponent and the butterfly velocity may be read off as follows

$$\lambda_L = \frac{2\pi}{\beta}, \quad v_B = \frac{2\pi}{\beta\mathcal{M}} = \sqrt{1 - \frac{8\pi^2\mu}{\beta^2}}. \quad (3.50)$$

It is easy to see that although for $\mu > 0$, the Mezei-Stanford bound (1.3) is satisfied, we see a clear violation of the bound for negative values of the deformation parameter [cf. Fig. 4], which allows for superluminal propagation of chaos in $\text{T}\bar{\text{T}}$ deformed theories. This result, although seemingly violating causality, is not very surprising. As discussed in [45,64], the signal propagation speed in $\text{T}\bar{\text{T}}$ deformed theories can become superluminal for⁷ $\mu < 0$, due to the repulsive nature of the particle interactions. This may also be understood as the $\text{T}\bar{\text{T}}$ deformation effectively placing the CFT on a curved manifold (cf. Sec. V and Appendix A 2), whose causal structure provides the notion of a rescaled butterfly velocity [64]. In fact, the bound $v_B \leq 1$ obtained in [101] for asymptotically AdS spacetimes obeying the null energy condition has been shown to be violated for nonlocal boundary theories [102,103] as well as anisotropic states [104,105]. Further supporting evidences of superluminal butterfly velocity may be found in [17,18,24] where the authors considered the OTOC in driven and quenched CFTs.

Interestingly, near the critical value of μ originating from the reality of the ground state energy, namely the Hagedorn bound [50,64,106]

⁷Note the difference in the convention regarding the signature of μ in [45,64] as compared to ours.

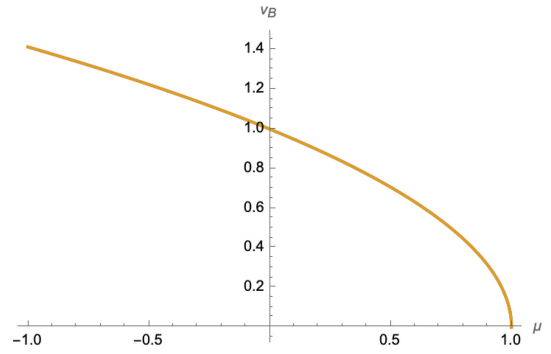


FIG. 4. Variation of the butterfly velocity with respect to the deformation parameter μ in the deformed BTZ black hole geometry. For $\mu < 0$, the butterfly velocity violated the bound derived in [5].

$$\mu < \mu_c = \frac{\beta^2}{8\pi}, \quad (3.51)$$

the butterfly velocity approaches zero, indicating hindered spread of chaos in $\text{T}\bar{\text{T}}$ -deformed theories. This phenomena, perhaps, also has its origin in the nonlocal nature of such theories [64].

C. Pole skipping

In this section, we wish to analyze the retarded energy density Green's function $G_{T_{00}T_{00}}^R(\omega, k)$ holographically, utilizing the techniques developed in [39,40]. This correlation function may be analyzed by perturbing the gravitational background and imposing ingoing boundary conditions near the horizon. It is customary to utilize the ingoing Eddington-Finkelstein coordinates

$$v = t + r_*, \quad dr_* = (1 + 2\mu\mathcal{L}_\mu) \frac{dr}{r^2 - 4\mathcal{L}_\mu}. \quad (3.52)$$

From Eq. (3.13), we may therefore obtain

$$v = t + \frac{1 + 2\mu\mathcal{L}_\mu}{4\sqrt{\mathcal{L}_\mu}} \log\left(\frac{r + 2\sqrt{\mathcal{L}_\mu}}{r - 2\sqrt{\mathcal{L}_\mu}}\right), \quad (3.53)$$

and subsequently the metric (3.2) may be written in the ingoing Eddington-Finkelstein (EF) gauge as follows

$$ds^2 = -(r^2 - 4L) \frac{dv^2}{(1 + 2\mu\mathcal{L}_\mu)^2} - \frac{2drdv}{1 + 2\mu\mathcal{L}_\mu} + r^2 \frac{dx^2}{(1 - 2\mu\mathcal{L}_\mu)^2}. \quad (3.54)$$

The action for 3d Einstein gravity is

$$S_{\text{EH}} = \frac{1}{16\pi G_N} \int d^3x \sqrt{-g} (R - 2\Lambda), \quad (3.55)$$

and the equations of motion following from the above action are given by (recall that Λ is related to the AdS radius as $\Lambda = -\frac{1}{\ell^2}$ and we set $\ell = 1$)

$$E_{\mu\nu} = R_{\mu\nu} - \frac{1}{2}g_{\mu\nu}R - g_{\mu\nu} = 0. \quad (3.56)$$

It is straightforward to verify that (3.54) satisfies (3.56).

To obtain the energy density Green's function in the momentum space, we now perturb the background metric by putting perturbations on the longitudinal modes or the sound modes. In particular, we choose the ansatz [39]

$$g_{\mu\nu} \rightarrow g_{\mu\nu} + h_{\mu\nu} = g_{\mu\nu} + \delta g_{\mu\nu}(r)e^{-i(\omega\nu - kx)}, \quad (3.57)$$

where $g_{\mu\nu}$ satisfies the vacuum Einstein's equations. Plugging the above ansatz into (3.56), we may obtain the field equations for $h_{\mu\nu}$ as follows [107]

$$E_{\mu\nu} = \nabla^\rho \nabla_{(\mu} h_{\nu)\rho} - \frac{1}{2} \nabla^\rho \nabla_\rho h_{\mu\nu} - \frac{1}{2} \nabla_\mu \nabla_\nu h - \frac{1}{2} g_{\mu\nu} \nabla^\rho \nabla^\sigma h_{\rho\sigma} + \frac{1}{2} g_{\mu\nu} \nabla^\rho \nabla_\rho h + 2h_{\mu\nu} - hg_{\mu\nu} = 0, \quad (3.58)$$

where $h = g^{\mu\nu} h_{\mu\nu}$. The above equation can also be obtained from the second order expansion of the Einstein-Hilbert action around the background (3.54) [107],

$$S = \frac{1}{16\pi G_N} \int d^3x \sqrt{-g} \left[2h_{\mu\nu} h^{\mu\nu} - h^2 - \frac{1}{2} (\nabla_\mu h) (\nabla^\mu h) + \frac{1}{2} (\nabla_\rho h_{\mu\nu}) (\nabla^\rho h^{\mu\nu}) + (\nabla_\mu h) (\nabla_\nu h^{\mu\nu}) - (\nabla_\nu h_{\mu\rho}) (\nabla^\rho h^{\mu\nu}) \right]. \quad (3.59)$$

The sound modes are given by

$$\delta g_{\nu\nu}, \delta g_{\nu x}, \delta g_{\nu r}, \delta g_{rr}, \delta g_{rx}, \delta g_{xx}.$$

Imposing radial gauge condition $\delta g_{r\mu} = 0$ and from the traceless condition $g^{\mu\nu} \delta g_{\mu\nu} = 0$, the nonredundant modes are only

$$\delta g_{\nu\nu}, \delta g_{\nu x}.$$

Furthermore, the perturbed equations should be regular at the horizon in the ingoing EF coordinates. Therefore, we expand the modes near the horizon as follows

$$\delta g_{\mu\nu}(r) = \delta g_{\mu\nu}^{(0)} + (r - 2\sqrt{\mathcal{L}_\mu}) \delta g_{\mu\nu}^{(1)} + \dots \quad (3.60)$$

As described in [39], the near horizon expansion of the linearized Einstein's equation $\delta E_{\nu\nu} = 0$ becomes degenerate at the special points (1.4), admitting an extra ingoing

mode and causing coincident zeros and poles in the retarded Green's function of the energy-density correlator [39]. This links the chaos parameters, the Lyapunov exponent λ_L and butterfly velocity v_B , directly to the analytic structure of thermal two-point functions, a feature verified in both anisotropic plasma models [41] and massive gravity backgrounds [108]. Thus, the Einstein equation, and its generalizations to other bulk fields, provides a universal gravitational origin for quantum chaos in holography. We may expand the Einstein's equations near the horizon using Eq. (3.60) for the perturbed sound modes Eq. (3.57). Expanding the linearized Einstein equation $\delta E_{\nu\nu} = 0$ near the horizon, we find the constraint relation

$$2k(1 - 2\mu\mathcal{L}_\mu)^2 \left(2\mu\mathcal{L}_\mu\omega - 2i\sqrt{\mathcal{L}_\mu} + \omega \right) \delta g_{\nu x}^{(0)} + (1 + 2\mu\mathcal{L}_\mu) \left(k^2(1 - 2\mu\mathcal{L}_\mu)^2 - 2i\sqrt{\mathcal{L}_\mu}\omega(1 + 2\mu\mathcal{L}_\mu) \right) \delta g_{\nu\nu}^{(0)} = 0. \quad (3.61)$$

Equating the coefficients of $\delta g_{\nu x}$ and $\delta g_{\nu\nu}$ separately to zero, we may obtain the pole skipping points as follows

$$(\omega_\star, k_\star) = \left(i \frac{2\sqrt{\mathcal{L}_\mu}}{1 + 2\mu\mathcal{L}_\mu}, i \frac{2\sqrt{\mathcal{L}_\mu}}{1 - 2\mu\mathcal{L}_\mu} \right) = \left(i \frac{2\pi}{\beta}, i \frac{2\pi}{\sqrt{\beta^2 - 8\pi^2\mu}} \right). \quad (3.62)$$

Therefore, from Eq. (1.4) we obtain the same values for the Lyapunov exponent and the butterfly velocity, as computed from the shock wave method and OTOC.

D. Entanglement wedge method

In this section, we aim to find the butterfly velocity utilizing the entanglement wedge method [5]. We are required to calculate the size of the smallest boundary region for which the falling particle is contained in the entanglement wedge as depicted in Fig. 5. At late times, the RT surface approaches the near-horizon region and exhibits a characteristic profile, which propagates outward at a constant velocity. As described in [34,35], the holographic entanglement entropy can be obtained in terms of the area of the minimal codimension-two surface (dubbed the RT surface) homologous to the subsystem under consideration. This RT surface is determined by extremizing the area functional

$$\mathcal{A} = 2\pi \int_\Gamma d^{d-1}y \sqrt{\gamma}, \quad (3.63)$$

where γ is the determinant of the induced metric on a codimension-two hypersurface Γ described by the coordinates y . For a constant time slice of the deformed BTZ

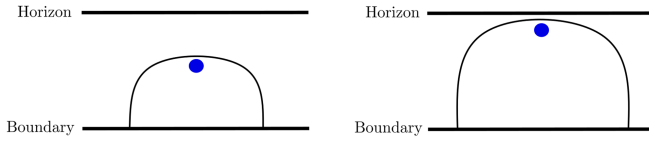


FIG. 5. Falling particle being enclosed in the entanglement wedge of a boundary region that grows with the butterfly velocity.

black hole background in Eq. (3.2), the induced metric on Γ is given by

$$\gamma_{ab} dx^a dx^b = \frac{1}{z^2(x)} \left[\frac{z'(x)^2}{1 - 4\mathcal{L}_\mu z(x)^2} + \frac{1}{(1 - 2\mu\mathcal{L}_\mu)^2} \right] dx^2, \quad (3.64)$$

where we have parametrized Γ as $z = z(x)$ with $z = \frac{1}{r}$. The equation of the RT surface is given by the Euler-Lagranges equation for the area functional (3.63),

$$\frac{z(x)(4\mathcal{L}_\mu z(x)^2 - 1)z''(x) + (1 - 8\mathcal{L}_\mu z(x)^2)z'(x)^2}{(1 - 4\mathcal{L}_\mu z(x)^2)^2} = \frac{1}{(1 - 2\mu\mathcal{L}_\mu)^2}. \quad (3.65)$$

As we work in the near horizon region, we will make the following ansatz for the RT profile [5,109],

$$z(x) = 2\sqrt{\mathcal{L}_\mu} - \epsilon s(x)^2, \quad (3.66)$$

where ϵ is a small parameter and $s(x)$ quantifies the closeness of the RT surface and the horizon. We may Taylor expand the equation of motion around $\epsilon = 0$, to obtain the following differential equation for the RT profile⁸

$$s''(x) - \frac{4\mathcal{L}_\mu}{(1 - 2\mu\mathcal{L}_\mu)^2} s(x) = 0 \Rightarrow s(x) = e^{\frac{2\sqrt{\mathcal{L}_\mu}}{1 - 2\mu\mathcal{L}_\mu} x}. \quad (3.68)$$

At any point of time, we demand that the tip of the RT surface intersects the particle, which is enforced by setting [5]

$$s(x=0, t) \sim e^{-\frac{2\pi t}{\beta}}. \quad (3.69)$$

⁸Alternatively, we may also Taylor expand the induced metric γ near the horizon to obtain

$$\gamma_{ab} dx^a dx^b = \left[\frac{4\mathcal{L}_\mu}{(1 - 2\mu\mathcal{L}_\mu)^2} + 4\epsilon\sqrt{\mathcal{L}_\mu} \left(\frac{4\mathcal{L}_\mu}{(1 - 2\mu\mathcal{L}_\mu)^2} s(x)^2 + s'(x)^2 \right) \right]. \quad (3.67)$$

Taking the variation of the determinant $\sqrt{\gamma}$, we obtain the same differential equation (3.68) for the RT profile $s(x)$.

Using Eqs. (3.68) and (3.69), the time dependent RT profile for the boundary region is given by

$$s(x, t) \sim e^{\frac{2\sqrt{\mathcal{L}_\mu}}{1 - 2\mu\mathcal{L}_\mu} x - \frac{2\pi t}{\beta}}. \quad (3.70)$$

At any given time t , there is some size of the boundary region $x = x_\star = \tilde{v}_B t$ such that $s(x_\star, t) \sim \mathcal{O}(1)$. This gives the minimal size of the boundary region, which propagates outward with a characteristic velocity

$$\tilde{v}_B = \frac{2\pi}{\beta} \frac{1 - 2\mu\mathcal{L}_\mu}{2\sqrt{\mathcal{L}_\mu}} = \sqrt{1 - \frac{8\pi^2\mu}{\beta^2}}, \quad (3.71)$$

which clearly aligns with our result for the butterfly velocity in (3.50). Therefore, the entanglement wedge method also corroborates our finding related to the violation of the Mezei-Stanford bound for $\mu < 0$.

IV. ROTATING BTZ

Having established the robustness of the three methods in characterizing chaos properties, namely the shock wave method, pole skipping, and the entanglement wedge method, for the TT̄ deformed nonrotating BTZ black hole, we now address the issue of characterizing chaos properties of the deformed rotating black holes. As discussed earlier, the entanglement wedge method is only reliable for static geometries in the bulk, it is not suitable for the rotating case and we restrict our attention to the shock wave analysis and the pole skipping phenomena.

A. Pole skipping

As we have already seen, the shock wave and OTOC calculations lead to same characteristics of chaos,⁹ in this section we will restrict ourselves to the investigation of the pole skipping phenomena in the rotating black hole case. In the Fefferman-Graham gauge, the deformed rotating black hole spacetime is given by [81]

$$ds^2 = \frac{d\rho^2}{4\rho^2} + \frac{1 + 4\mu^2\mathcal{L}_\mu\bar{\mathcal{L}}_\mu + \rho\mathcal{L}_\mu\bar{\mathcal{L}}_\mu(\rho + 8\mu + 4\mu^2\mathcal{L}_\mu\bar{\mathcal{L}}_\mu\rho)}{\rho(1 - 4\mu^2\mathcal{L}_\mu\bar{\mathcal{L}}_\mu)^2} dZd\bar{Z} + \frac{(\rho + 2\mu)(1 + 2\mu\mathcal{L}_\mu\bar{\mathcal{L}}_\mu\rho)}{\rho(1 - 4\mu^2\mathcal{L}_\mu\bar{\mathcal{L}}_\mu)^2} (\mathcal{L}_\mu dZ^2 + \bar{\mathcal{L}}_\mu d\bar{Z}^2). \quad (4.1)$$

⁹Note that in the rotating case, there are various subtleties related to the wrong choice of affine parametrization and null coordinates due to the presence of an angular momentum of the rotating shock wave, which makes the Kruskal extension subtle and correspondingly the shock wave calculations are cumbersome. See for example, [16,110,111]. In this article, we refrain from considering rotating shock waves.

Defining the new variables

$$r^2 = \frac{1}{\rho} + \mathcal{L}_\mu + \bar{\mathcal{L}}_\mu + \rho \mathcal{L}_\mu \bar{\mathcal{L}}_\mu, \quad Z = x + t, \quad \bar{Z} = x - t, \quad (4.2)$$

the above metric may be recast in the following form [91]

$$ds^2 = \frac{r^2}{(r^2 - r_+^2)(r^2 - r_-^2)} dr^2 - (r^2 - r_+^2) \frac{(r_+ dt - r_- dx)^2}{r_h^2 \left(1 + \frac{r_h^2}{2} \mu\right)^2} + (r^2 - r_-^2) \frac{(r_+ dx - r_- dt)^2}{r_h^2 \left(1 - \frac{r_h^2}{2} \mu\right)^2}, \quad (4.3)$$

where we have used the notations

$$\mathcal{L}_\mu = \frac{1}{4}(r_+ - r_-)^2, \quad \bar{\mathcal{L}}_\mu = \frac{1}{4}(r_+ + r_-)^2, \quad r_h^2 = r_+^2 - r_-^2. \quad (4.4)$$

This geometry is dual to a $\text{T}\bar{\text{T}}$ -deformed CFT_2 at a finite temperature β^{-1} and chemical potential for angular momentum Ω given by [91]

$$\beta = \frac{\pi}{2} \left(\frac{1}{\sqrt{\mathcal{L}_\mu}} + \frac{1}{\sqrt{\bar{\mathcal{L}}_\mu}} \right) (1 + 2\mu \sqrt{\mathcal{L}_\mu \bar{\mathcal{L}}_\mu}), \quad \Omega = \frac{\sqrt{\bar{\mathcal{L}}_\mu} - \sqrt{\mathcal{L}_\mu}}{\sqrt{\bar{\mathcal{L}}_\mu} + \sqrt{\mathcal{L}_\mu}}. \quad (4.5)$$

For the near horizon analysis, it is convenient to use the comoving coordinates (r, t, ϕ) where

$$\phi = x - \frac{r_-}{r_+} t \equiv x - \Omega t, \quad (4.6)$$

in which the metric reads

$$ds^2 = \frac{r^2}{(r^2 - r_+^2)(r^2 - r_-^2)} dr^2 - \frac{(r^2 - r_+^2)}{r_h^2 \left(1 + \frac{r_h^2}{2} \mu\right)^2} \left(\frac{r_h^2}{r_+} dt - r_- d\phi \right)^2 + (r^2 - r_-^2) \frac{r_+^2 d\phi^2}{r_h^2 \left(1 - \frac{r_h^2}{2} \mu\right)^2}. \quad (4.7)$$

In these coordinates, the angular speed vanishes at the horizon $\Omega_H = 0$. These two theories are related by the boost transformation (4.6). The momentum variables in the comoving and Schwarzschild coordinates are related by [107]

$$\omega_{\text{Sch}} = \omega_{\text{cm}} + \Omega k_{\text{cm}}, \quad k_{\text{Sch}} = k_{\text{cm}}. \quad (4.8)$$

In order to analyze ingoing boundary conditions near the horizon, it is customary to use the ingoing Eddington-Finkelstein coordinates. The ingoing EF time \mathfrak{v} can be obtained from the comoving metric as

$$\mathfrak{v} = t + r_\star, \quad dr_\star = \frac{rr_+(2 + r_h^2 \mu)}{2r_h \sqrt{r^2 - r_-^2} (r^2 - r_+^2)}, \quad (4.9)$$

where the tortoise coordinate is given by

$$r_\star = \frac{r_+(1 + \frac{r_h^2}{2} \mu)}{2r_h^2} \log \left[\frac{\sqrt{r^2 - r_-^2} - r_h}{\sqrt{r^2 - r_-^2} + r_h} \right]. \quad (4.10)$$

Therefore, the deformed metric in the ingoing EF coordinates can be written as

$$\begin{aligned}
ds^2 = & -\frac{(r^2 - r_+^2)r_h^2}{r_+^2\left(1 + \frac{r_h^2}{2\mu}\right)^2} dv^2 + 2\frac{rr_h}{r_+\sqrt{r^2 - r_-^2}} \frac{dvdr}{\left(1 + \frac{r_h^2}{2\mu}\right)} + 2\frac{r_-}{r_+} (r^2 - r_+^2) \frac{dv d\phi}{\left(1 + \frac{r_h^2}{2\mu}\right)^2} \\
& -\frac{2rr_-}{r_h\sqrt{r^2 - r_-^2}} \frac{dr d\phi}{\left(1 + \frac{r_h^2}{2\mu}\right)} + \frac{4(-8r_-^2 r_+^2 \mu + r^2(4 + 4(r_+^2 + r_-^2)\mu + r_h^4 \mu^2))}{(4 - r_h^4 \mu^2)^2} d\phi^2.
\end{aligned} \tag{4.11}$$

To proceed, we assume that the angular coordinate ϕ is noncompact, namely, we are working in the high temperature limit. We now allow for the perturbations on the longitudinal modes, as in Eq. (3.57) and expand the fields near the (outer) horizon¹⁰

$$\delta g_{\mu\nu} = \sum_{n=0}^{\infty} \delta g_{\mu\nu}^{(n)} (r - r_+)^n. \tag{4.12}$$

Then the vv component of the Einstein's equations, in the leading order about the (outer) horizon, results in the following constraint equation

$$\begin{aligned}
r_+(-k(2 - \mu r_h^2)^2(-k(\mu r_h^2 + 2) + 4ir_-) - 2ir_+\omega(\mu(r_- - r_+)^2 + 2)(\mu(r_- + r_+)^2 + 2))\delta g_{vv}^{(0)} \\
+ 2k(2 - r_h^2 \mu)^2(\omega r_+(2 + r_h^2 \mu) - 2ir_h^2)\delta g_{vx}^{(0)} = 0.
\end{aligned} \tag{4.13}$$

Setting the coefficients of δg_{vx} , δg_{vv} to zero separately, we obtain the pole skipping points as follows

$$\begin{aligned}
(\omega_\star, k_\star) &= \left(\frac{2ir_h^2}{r_+(2 + r_h^2 \mu)}, \pm \frac{2i(r_+ \pm r_-)(2 + (r_+ \mp r_-)^2 \mu)}{4 - r_h^4 \mu^2} \right), \\
&= \left(\frac{2\pi i}{\beta}, \pm \frac{2\pi i}{\beta(1 - \Omega^2)} \left(\Omega \pm \frac{1}{\sqrt{1 - \frac{8\pi^2 \mu}{\beta_+ \beta_-}}} \right) \right),
\end{aligned} \tag{4.14}$$

where in the second equality, we have used Eqs. (4.4) and (4.5) to express the horizon radii in terms of the field theoretic parameters β, Ω . It should be emphasized that the other components of the Einstein's equations are regular at these points. From the above expression, using Eq. (1.4), we may infer the chaos parameters as follows

$$\lambda_L = \frac{2\pi}{\beta}, \quad v_B = \pm \frac{1 - \Omega^2}{\Omega \pm \frac{1}{\sqrt{1 - \frac{8\pi^2 \mu}{\beta_+ \beta_-}}}}. \tag{4.15}$$

Therefore, in the comoving coordinates, the Lyapunov exponent saturates the MSS bound. We plot the butterfly velocities in Fig. 6. Interestingly, the butterfly velocity in the comoving coordinates seem to vanish at some particular value of μ ,

$$\mu_{\text{Hagedom}} = \frac{\beta^2(1 - \Omega^2)}{8\pi^2} \equiv \frac{\beta_+ \beta_-}{8\pi^2}. \tag{4.16}$$

However, this value corresponds to the spinning analog of the Hagedorn bound [64,91], where the $\text{T}\bar{\text{T}}$ deformed energy levels become complex and hence do not correspond to a physically relevant situation. Note that, as $\Omega \rightarrow 0$, we find $v_B = \sqrt{1 - \frac{8\pi^2 \mu}{\beta^2}}$, thereby reproducing the nonrotating result (3.50). Furthermore, as $\mu \rightarrow 0$, we reproduce the undeformed results obtained in [112]

$$\lambda_L = \frac{2\pi}{\beta}, \quad v_B = 1 \pm \Omega. \tag{4.17}$$

¹⁰Note that, remarkably the Einstein's equations are regular at the inner horizon.

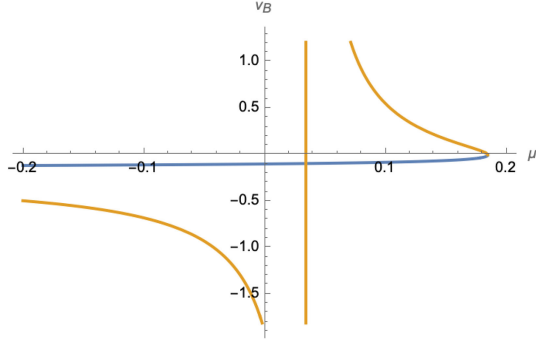


FIG. 6. Variation of the butterfly velocity with respect to μ in the comoving coordinates.

In the Schwarzschild coordinates, the transformed frequencies are obtained from Eq. (4.8)

$$(\omega_{\star}, k_{\star}) = \left(\frac{2\pi i}{\beta(1-\Omega^2)} \left(1 \pm \frac{\Omega}{\sqrt{1 - \frac{8\pi^2\mu}{\beta^2(1-\Omega^2)}}} \right), \right. \\ \left. \pm \frac{2\pi i}{\beta(1-\Omega^2)} \left(\Omega \pm \frac{1}{\sqrt{1 - \frac{8\pi^2\mu}{\beta_+\beta_-}}} \right) \right), \quad (4.18)$$

from which we may read off the chaos parameters as follows

$$\lambda_L^{\pm} = \frac{2\pi}{\beta(1-\Omega^2)} \left(1 \mp \frac{\Omega}{\sqrt{1 - \frac{8\pi^2\mu}{\beta_+\beta_-}}} \right), \\ v_B^{\pm} = \frac{\Omega \pm \sqrt{1 - \frac{8\pi^2\mu}{\beta_+\beta_-}}}{1 \pm \Omega \sqrt{1 - \frac{8\pi^2\mu}{\beta_+\beta_-}}}. \quad (4.19)$$

Hence, similar to the undeformed case, we find two Lyapunov exponents corresponding to the left and right moving modes in the dual CFT₂ with T \bar{T} deformation. In Fig. 7, we have plotted the two Lyapunov exponents and

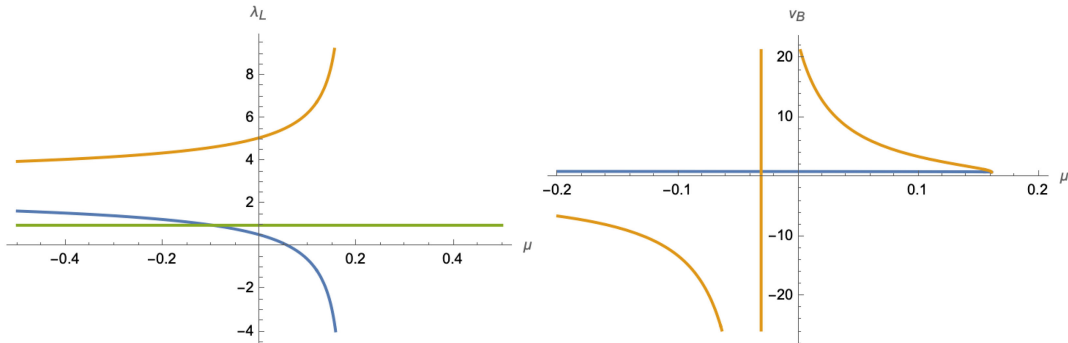


FIG. 7. Variation of the Lyapunov exponent and butterfly velocity with respect to μ in the Schwarzschild coordinates.

butterfly velocities with respect to the deformation parameter μ . Note that, once again, if we switch off the rotation of the black hole, the chaos parameters reduce to our earlier findings in (3.50).

We find that λ_L^- always seems to violate the chaos bound, similar to the undeformed case and it is necessary to take into account the periodicity of the ϕ coordinate to get rid of this pathology, as described in [113]. However, in the high temperature limit, λ_L^- does serve as the upper limit of the instantaneous Lyapunov exponent, which may be interpreted as the effective Lyapunov exponent corresponding to the right movers who find themselves immersed in a thermal ensemble at inverse temperature β_- . Interestingly, in the deformed case, we find that at some particular negative value of μ , given as

$$\mu_l = -\frac{\beta^2(1-\Omega^2)^2}{8\pi^2\Omega^2} \equiv -\frac{\beta_+^2\beta_-^2}{2\pi^2(\beta_+ - \beta_-)^2}, \quad (4.20)$$

even λ_L^+ starts to violate the chaos bound. However, as argued in [91,114], at this value of μ the T \bar{T} -deformed theory is not well defined. For example, the spacelike RT surface computing the entanglement entropy of a spatial subsystem in the field theory becomes null at this limit and correspondingly the entanglement entropy is IR divergent. Hence μ_l serves as a lower bound to the deformation parameter, and correspondingly there is no violation of the MSS bound from the left moving modes. Furthermore, at the Hagedorn temperature (4.16), both λ_L^{\pm} diverge indicating breakdown of the T \bar{T} deformed theory. Interestingly, in this limit, the butterfly velocities remains finite, and is equal to the angular speed of the black hole $v_B^{\pm}(\mu_{\text{Hagedorn}}) = \Omega$. This conforms with our earlier findings in the case of nonrotating black holes. Remarkably, in the range

$$\mu_l < \mu < 0, \quad (4.21)$$

the butterfly velocity v_B^+ exceeds the Mezei-Stanford bound. As discussed earlier, such behavior is already expected from the nonlocal nature of the T \bar{T} deformation.

1. Extremal black holes

We now briefly comment on the extremal black hole case, which corresponds to $r_- \rightarrow r_+$ or, alternatively $\Omega \rightarrow 1$, $\beta \rightarrow \infty$. The deformed black hole metric may be obtained from Eq. (4.1) by taking the limit $\mathcal{L}_\mu \rightarrow 0$ as follows

$$\begin{aligned} ds^2 &= \frac{d\rho^2}{4\rho^2} + \frac{1}{\rho} dZ d\bar{Z} + \left(1 + \frac{2\mu}{\rho}\right) \bar{\mathcal{L}}_\mu d\bar{Z}^2 \\ &= \frac{r^2 dr^2}{(r^2 - r_0^2)^2} + 2(r^2 - r_0^2) dt d\phi \\ &\quad + (2\mu r^2 r_0^2 + r^2 - 2\mu r_0^4) d\phi^2 \end{aligned} \quad (4.22)$$

where, in the second equality, we have made the following change of coordinates

$$r^2 = \frac{1}{\rho} + \bar{\mathcal{L}}_\mu, \quad Z = \phi + 2t, \quad \bar{Z} = \phi. \quad (4.23)$$

In this case, we find that the Lyapunov exponent and the butterfly velocity both vanish for the right moving modes, whereas for the left moving modes they are independent of the deformation parameter,

$$\lambda_L^{\text{ext}} = \frac{2\pi}{\beta_{\text{FT}}}, \quad v_B^{\text{ext}} = 1, \quad (4.24)$$

where $\beta_{\text{FT}} = \frac{\pi}{r_0}$ corresponds to the effective Frolov-Thorne temperature. This is surprising, since the deformed metric (4.22) is still dependent on μ in the extremal limit and warrants further investigation.

B. shock waves and OTOC

In this subsection, we present a brief account of the shock wave solutions in TT̄ deformed rotating BTZ black holes and the corresponding OTOC computations. The maximal Kruskal extension of the deformed rotating BTZ black hole

may be obtained utilizing the comoving coordinates (4.7) and the tortoise coordinate (4.10) as follows

$$u = -e^{-\kappa u} \equiv -e^{-\kappa(t-r_*)}, \quad v = e^{\kappa u} \equiv e^{\kappa(t+r_*)}, \quad (4.25)$$

with the surface gravity¹¹

$$\kappa = \frac{r_+^2 - r_-^2}{r_+ [1 + \frac{1}{2}\mu(r_+^2 - r_-^2)]} = \frac{2\pi}{\beta}, \quad (4.27)$$

where in the second equality, we have made use of Eqs. (4.4) and (4.5). In these coordinates, the deformed black hole metric (4.7) takes the form

$$\begin{aligned} ds^2 &= -\frac{4dudv}{(1+uv)^2} - \frac{4r_-(udv - vdu)d\phi}{(1 + \frac{r_-}{2}\mu)(1+uv)^2} \\ &\quad + \frac{1}{(1+uv)^2} \left[\frac{4r_-^2 uv}{(1 + \frac{r_-}{2}\mu)^2} + \frac{r_+^2 (1-uv)^2}{(1 - \frac{r_+}{2}\mu)^2} \right] d\phi^2. \end{aligned} \quad (4.28)$$

We consider perturbing the above solution with the insertion of a localized shock wave

$$T_{uu}^{\text{shock}} = E_0 e^{\kappa t} \delta(u) \delta(\phi), \quad (4.29)$$

localized on the horizon $u = 0$ at $\phi = 0$. Here, E_0 is a constant related to the asymptotic energy of the shock wave and $e^{\kappa t}$ represents the blueshift factor. This has the following effect on the metric [95,97]

$$ds^2 \rightarrow ds^2 + \frac{2}{(1+uv)^2} \delta(u) h(\phi) du^2, \quad (4.30)$$

where $h(\phi)$ quantifies the shift in the horizon after shock wave insertion. Note that the transverse directions are unaffected by the shock wave. Then the uu component of the Einstein equation leads to the following differential equation

$$\begin{aligned} &(\mu(r_-^2 - r_+^2) - 2)(\mu(r_-^2 - r_+^2) + 2)^2 (h''(\phi)(\mu(r_-^2 - r_+^2) - 2) + 4r_- h'(\phi)) \\ &\quad + 4h(\phi)(r_-^2 - r_+^2)(\mu^2 r_+^4 - 2\mu r_-^2(\mu r_+^2 - 2) + (\mu r_+^2 + 2)^2) = 8\pi G_N E_0 e^{\kappa t} \delta(\phi). \end{aligned} \quad (4.31)$$

The general solution to the above equation is given by

$$\begin{aligned} h(\phi) &= c_1 e^{\kappa t} e^{\frac{(r_+ + r_-)(1 + \frac{\mu}{2}(r_+ - r_-)^2)}{1 - \frac{\mu}{4}(r_+^2 - r_-^2)^2}} + c_2 e^{\kappa t} e^{\frac{(r_+ - r_-)(1 + \frac{\mu}{2}(r_+ + r_-)^2)}{1 - \frac{\mu}{4}(r_+^2 - r_-^2)^2}}, \\ &= c_1 \exp \left[\frac{2\pi}{\beta} \left(t - \frac{\Omega + \frac{1}{\sqrt{1 - \frac{8\pi^2 \mu}{\beta_+ \beta_-}}}}{1 - \Omega^2} \phi \right) \right] + c_2 \exp \left[\frac{2\pi}{\beta} \left(t + \frac{\Omega - \frac{1}{\sqrt{1 - \frac{8\pi^2 \mu}{\beta_+ \beta_-}}}}{1 - \Omega^2} \phi \right) \right], \end{aligned} \quad (4.32)$$

¹¹The surface gravity in the deformed rotating BTZ geometry (4.3) may be computed from the Killing vector $\xi = \partial_t$ as follows

$$\kappa^2 = -\frac{1}{2} (\nabla_\mu \xi_\nu) (\nabla^\mu \xi^\nu)|_{r=r_+}. \quad (4.26)$$

where we have absorbed the step functions inside the coefficients $c_{1,2}$. Remarkably, identifying the shock wave profile with the OTOC, we find that the shock wave analysis leads to the same chaos parameters as obtained from the pole skipping analysis in Eq. (4.15).

1. Periodicity of ϕ

As discussed earlier, the above analysis is only true for the case in which the angular direction ϕ is noncompact, that is in the high temperature limit. As described in [113,115], for finite temperatures, the correct interpretation of the behavior of OTOC requires taking into account the periodicity of the function $h(\phi)$. In the following, we will show that the above behavior is reproduced in the high temperature limit of the correct Lyapunov exponent.

We impose the periodicity by replacing $h(\phi) \rightarrow h(\phi \bmod 2\pi)$. This may be achieved by replacing $\delta(\phi)$ with $\sum_{n=0}^{\infty} \delta(\phi - 2\pi n)$ in Eq. (4.31) (see, e.g., [113,115]). Therefore, restricting the domain of ϕ as $\phi \in [0, 2\pi)$, we obtain the solution

$$\begin{aligned} h(\phi) &= e^{\kappa t} \left[\sum_{n=-\infty}^0 e^{\frac{2\pi(\phi-2\pi n)}{\beta v_{\pm}^{\pm}}} + \sum_{n=1}^{\infty} e^{\frac{2\pi(\phi-2\pi n)}{\beta v_{\pm}^{\pm}}} \right], \\ &= e^{\kappa t} \left[\frac{e^{-\frac{2\pi}{\beta v_{\pm}^{\pm}} \phi(\bmod 2\pi)}}{1 - e^{-\frac{4\pi^2}{\beta v_{\pm}^{\pm}}}} + \frac{e^{\frac{2\pi}{\beta v_{\pm}^{\pm}} \phi(\bmod 2\pi)}}{e^{\frac{4\pi^2}{\beta v_{\pm}^{\pm}}} - 1} \right], \end{aligned} \quad (4.33)$$

where we have denoted

$$v_B^{\pm} = \pm \frac{1 - \Omega^2}{\Omega \pm \frac{1}{\sqrt{1 - \frac{8\pi^2 \mu}{\beta_+ \beta_-}}}}. \quad (4.34)$$

We have plotted the function $h(\phi)$ for different values of μ in Fig. 8. Now the OTOC may be computed using the following expression¹² [113]

$$f(t, x) = 1 - \epsilon_{VW} h(\Omega t - x), \quad (4.35)$$

which is governed by two sets of exponents and the corresponding velocities. In Fig. 9, we plot the OTOC with respect to time keeping x constant. The function grows as $e^{2\pi t/\beta}$ with a periodic modulation for different values of the deformation parameter. Notice the unusual feature for $\mu_l < \mu < 0$, where the modulation grows beyond the chaos bound, as compared to the undeformed case discussed in [115]. However, we find that the

¹²Note that our definition of the OTOC misses a factor of $e^{\kappa t}$ as compared to [113], since in our conventions $h(\phi)$ already carries the same prefactor.

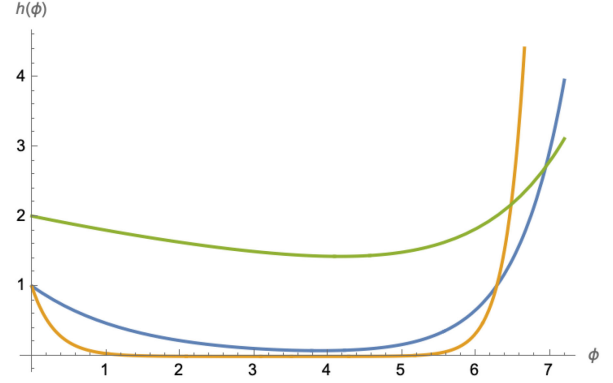


FIG. 8. Shock profile in deformed rotating BTZ geometry. We have set $\Omega = \frac{1}{3}$, $\beta = 2\pi$ and $\mu = 0$ (blue), 0.4 (yellow), -1.95 (green).

average Lyapunov exponent still saturates the chaos bound¹³

$$\bar{\lambda}_L = \frac{2\pi}{\beta}. \quad (4.37)$$

2. Instantaneous Lyapunov exponent

In Fig. 10, we plot the instantaneous Lyapunov exponent [115], defined as follows

$$\lambda_{\text{inst}}(t) = \frac{|\partial_t f(t, 0)|}{1 - f(t, 0)} = \frac{2\pi}{\beta} + \frac{\partial_t h(\Omega t)}{h(\Omega t)}. \quad (4.38)$$

Notice that in the presence of deformation, we cannot go to arbitrarily high temperatures beyond the Hagedorn bound for $\mu > 0$ and observe the step function behavior of λ_{inst} . However as seen in the right panel of Fig. 10, for small values of μ , the high temperature behavior (below the Hagedorn temperature $\beta_{\text{Hagedorn}} = \sqrt{\frac{8\pi^2 \mu}{1 - \Omega^2}}$) shows a sharp transition between the values λ_L^{\pm} reported in (4.19).

Furthermore, it is easy to verify that

$$\left| \frac{(\partial_t + \Omega \partial_x) f(t, x)}{1 - f(t, x)} \right| = \frac{2\pi}{\beta}. \quad (4.39)$$

Therefore, the OTOC saturates the modified chaos bound for the ‘‘Hamiltonian’’ $\beta(H + \Omega J)$ in the rotating ensemble, even in the presence of the nonlocal $\text{T}\bar{\text{T}}$ deformation [115].

¹³The average Lyapunov exponent is defined as the time average of the instantaneous Lyapunov exponent over the periodic time $\frac{2\pi}{\Omega}$.

$$\bar{\lambda}_L = \frac{\Omega}{2\pi} \int_0^{\frac{2\pi}{\Omega}} \lambda_{\text{inst}}(t) dt. \quad (4.36)$$

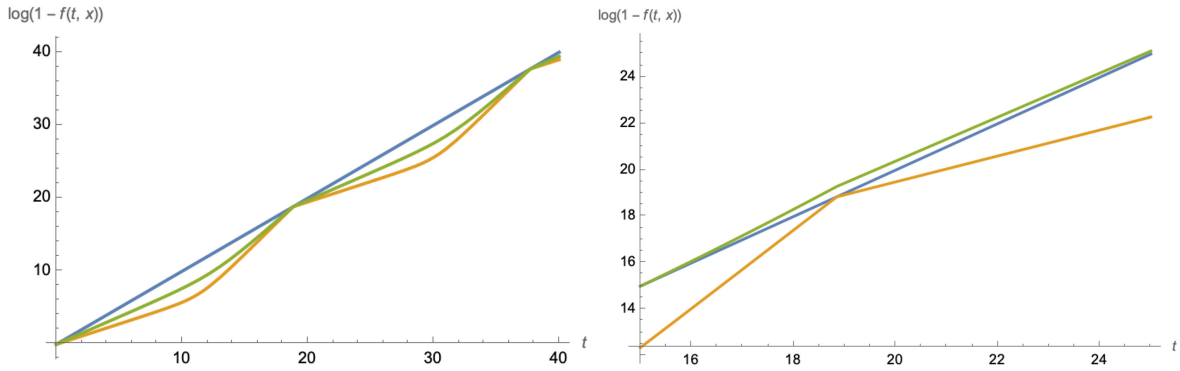


FIG. 9. Modulation of the OTOC for different deformation parameters. In the right panel, for $\mu < 0$, the modulation grows beyond the chaos bound, shown by the blue curve. The average Lyapunov exponent still saturates the bound $\bar{\lambda}_L = \frac{2\pi}{\beta}$. We have set $\beta = 2\pi$, $\Omega = \frac{1}{3}$ and (left panel) $\mu = 0$ (yellow), 0.25 (green); (right panel) $\mu = 0$ (yellow), -1.5 (green).

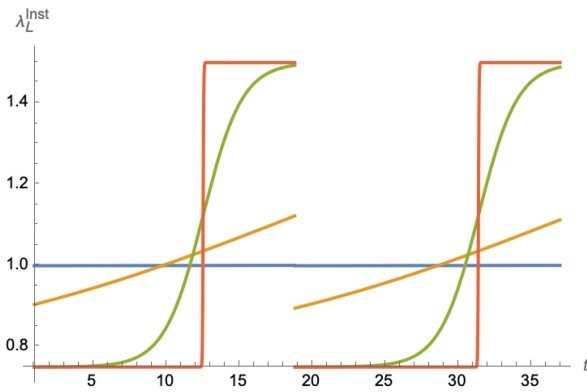


FIG. 10. Instantaneous Lyapunov exponent with respect to time. (Left panel) $\mu = 0$, (right panel) $\mu = 0.05$. We have set $\Omega = \frac{1}{3}$ and plotted λ_{inst} for different values of $\beta = 0, 2\pi, 20\pi, \infty$ (left panel) and $\beta = \pi, 2\pi, 20\pi, \lesssim \beta_{\text{Hagedorn}}$ (right panel).

V. CONNECTION WITH THE CUTOFF PRESCRIPTION

In this section, we comment on the connection of our holographic computations in the mixed boundary conditions prescription with the cutoff prescription of [64]. The important point to note is that in order to interpret the radial cutoff in terms of the deformation parameter, one must consider the black hole belonging to the deformed phase space [81], namely those obeying the nonlinear mixed boundary conditions (2.7). The authors in [64] chose to work with Brown-Henneaux asymptotics, and hence the conserved charges as obtained from the undeformed metric do not align with those in the deformed field theory. We begin with the undeformed (nonrotating) BTZ black hole with metric

$$ds^2 = -(r^2 - r_h^2)dt^2 + \frac{dr^2}{r^2 - r_h^2} + r^2 dx^2. \quad (5.1)$$

The induced metric at the cutoff surface $r = r_c$ is given by

$$ds^2 = (r_c^2 - r_h^2) \left(-dt^2 + \frac{dx^2}{1 - \frac{r_h^2}{r_c^2}} \right) := (r_c^2 - r_h^2) (-dt^2 + d\tilde{x}^2), \quad (5.2)$$

where the conformal spatial coordinate is given as [116,117]

$$\tilde{x} = x \left(1 - \frac{r_h^2}{r_c^2} \right)^{-1/2}. \quad (5.3)$$

Recall that in the cutoff prescription, the cutoff radius in the bulk is related to the deformation parameter μ in the boundary theory, in our conventions, as follows [64,116,117]

$$r_c^2 = -\frac{1}{2\mu}. \quad (5.4)$$

We now transform to the Fefferman-Graham gauge (2.8) with $\mathcal{L}_\mu = \tilde{\mathcal{L}}_\mu$ replaced by $\mathcal{L}_0 = \tilde{\mathcal{L}}_0 = \frac{r_h^2}{4}$, indicating that we are working with undeformed geometries as in [64]. In order to make a connection with the deformed theory, we utilize the relation between the deformed and undeformed parameters in the Fefferman-Graham gauge [81]

$$\mathcal{L}_0 = \frac{\mathcal{L}_\mu}{(1 - 2\mu\mathcal{L}_\mu)^2}. \quad (5.5)$$

Utilizing (3.3), we may now find that the rescaled spatial coordinate in (5.3) is given by

$$\tilde{x} = x \sqrt{1 - \frac{8\pi^2\mu}{\beta^2}}, \quad (5.6)$$

which is identical to the conformal spatial coordinate in the mixed boundary conditions (MBC) perspective (see, e.g.,

Appendix A 2). Therefore, all our bulk computations using the MBC picture may also be consistently reproduced from the cutoff picture. Note that, although the conformal factors are different in the two perspectives, we may ignore this discrepancy at least for the determination of chaos parameters.

In the case of the rotating BTZ black hole the equivalence between the cutoff and MBC pictures works in similar fashion. For simplicity, we proceed along the lines of [64]. The rotating BTZ black hole has the following metric in Schwarzschild coordinates

$$ds^2 = -f(r)dt^2 + \frac{dr^2}{f(r)} + r^2 \left(dx - \frac{r_+ r_-}{r^2} dt \right)^2, \quad f(r) = \frac{(r^2 - r_+^2)(r^2 - r_-^2)}{r^2}, \quad (5.7)$$

where r_{\mp} are the locations of the inner and outer horizons. Therefore, the induced metric at the $r = r_c$ surface may be written in a conformally flat form [64]

$$ds^2|_{r=r_c} = -f(r_c)dt^2 + r_c^2 \left(dx - \frac{r_+ r_-}{r_c^2} dt \right)^2 = r_c^2 (-dt_c^2 + dx_c^2), \quad (5.8)$$

with

$$dt_c = \frac{\sqrt{f(r_c)}}{r_c} dt, \quad dx_c = dx - \frac{r_+ r_-}{r_c^2} dt. \quad (5.9)$$

As described in [64], the signal propagation speed in the conformally flat coordinates (x_c, t_c) may be obtained by looking at the null trajectories in the (x, t) coordinates, leading to the relations

$$v_{\pm} = \frac{r_c \pm \frac{r_+ r_-}{r_c}}{\sqrt{f(r_c)}} = \frac{1 \mp 2\mu r_+ r_-}{\sqrt{1 + 2\mu(r_+^2 + r_-^2) + 4\mu^2 r_+^2 r_-^2}} \quad (5.10)$$

where, in the last equality, we have used the relation (5.4). Now, we may rewrite the above expression for the propagation speed in the deformed theory in terms of the Fefferman-Graham parameters $(\mathcal{L}_0, \bar{\mathcal{L}}_0)$ in the undeformed geometry, leading to

$$v_{\pm} = \frac{1 \mp 2\mu(\mathcal{L}_0 - \bar{\mathcal{L}}_0)}{\sqrt{1 + 4\mu(\mathcal{L}_0 + \bar{\mathcal{L}}_0) + 4\mu^2(\mathcal{L}_0 - \bar{\mathcal{L}}_0)^2}}. \quad (5.11)$$

This is identical to expression (4.19) for the signal propagation speed in [64], rewritten in our conventions. To derive the above expression, we have made use of the identities

$$J = r_+ r_- = \mathcal{L}_0 - \bar{\mathcal{L}}_0, \quad M = \frac{1}{2}(r_+^2 + r_-^2) = \mathcal{L}_0 + \bar{\mathcal{L}}_0. \quad (5.12)$$

Next, we use the following relations between the Fefferman-Graham parameters in the deformed and undeformed geometries [81]

$$\mathcal{L}_0 = \mathcal{L}_{\mu} \left(\frac{1 + 2\mu\bar{\mathcal{L}}_{\mu}}{1 - 4\mu^2\mathcal{L}_{\mu}\bar{\mathcal{L}}_{\mu}} \right)^2, \quad \bar{\mathcal{L}}_0 = \bar{\mathcal{L}}_{\mu} \left(\frac{1 + 2\mu\mathcal{L}_{\mu}}{1 - 4\mu^2\mathcal{L}_{\mu}\bar{\mathcal{L}}_{\mu}} \right)^2 \quad (5.13)$$

to find the signal propagation speed in terms of the deformed parameters as follows

$$v_+ = \frac{1 - 2\mu\mathcal{L}_{\mu}}{1 + 2\mu\mathcal{L}_{\mu}}, \quad v_- = \frac{1 - 2\mu\bar{\mathcal{L}}_{\mu}}{1 + 2\mu\bar{\mathcal{L}}_{\mu}}. \quad (5.14)$$

Finally, using the relation (4.5) between the deformed Fefferman-Graham parameters and the temperature and angular speed, it is straightforward to verify that the signal propagation speeds match identically with the butterfly velocities found in Eq. (4.19).

VI. SUMMARY AND DISCUSSIONS

To summarize, we have performed a detailed investigation of quantum chaos in the context of holographic $\overline{\text{T}\overline{\text{T}}}$ deformed theories by focusing on both nonrotating and rotating BTZ black holes in the bulk dual described in [81]. In particular, we considered three complementary methods such as shock wave geometries, pole skipping phenomena, and the entanglement wedge approach to characterize the chaos parameters, namely the Lyapunov exponent (λ_L) and the butterfly velocity (v_B). In this context, we first consider the deformed nonrotating BTZ black hole geometry, which can be written in Kruskal coordinates. Later, we introduce small perturbation to the corresponding geometry by adding few particles of very small energy from the left asymptotic boundary. This perturbation, while infinitesimal at early times, becomes an enormous blueshift as it approaches the horizon and backreacts to produce a gravitational shock wave. Utilizing the matching conditions across the null surface in the corresponding geometry, we obtained the backreacted metric in closed form, which is valid up to leading order in small energy.

We performed a holographic computation of OTOC by determining the geodesic lengths in a nonrotating deformed BTZ black hole geometry in Kruskal coordinates for both spherically symmetric and localized shock wave scenarios. Additionally, we verified the chaos parameters from two different methods namely the pole skipping and entanglement wedge method, which are consistent with our corresponding results. We extend our exploration of the

holographic chaos to the deformed rotating BTZ black hole case. In this regard, we mainly focused on the shock wave method for the study of OTOC and the pole skipping phenomena. We find that our results of the chaos parameters are consistent with the earlier literature [16,113] when the deformation μ is zero. Recently, in [118], the authors have argued that three independent probes of quantum chaos in holographic theories, namely pole skipping, shock wave-based OTOCs, and entanglement-wedge reconstruction, are in fact manifestations of the same underlying gravitational perturbation. More precisely, the pole skipping mode, when added to a black hole background, directly corresponds to the gravitational replica manifold used to compute the late-time entanglement wedge, while its imaginary component is precisely the horizon shock wave governing OTOC behavior. However, it is important to note that the RT prescription in holographic $T\bar{T}$ -deformed geometries lacks a rigorous derivation to date (a heuristic argument in the context of the cutoff prescription is presented in [119]); consequently, the equivalence between the three chaos diagnostics is not guaranteed *a priori* in such settings.

Interestingly for the nonrotating BTZ black hole, we observed that the Lyapunov exponent ($\lambda_L = \frac{2\pi}{\beta}$), obtained from pole skipping points and OTOCs in the shock wave geometry is independent of the deformation parameter μ and saturates the Maldacena-Shenker-Stanford bound described in [37]. In the rotating case, the comoving coordinates yield a Lyapunov exponent that saturates the MSS bound. However in Schwarzschild coordinates, the left- and right-moving modes exhibit distinct exponents, with λ_L^- potentially violating the bound unless periodicity on the ϕ coordinate is enforced. This behavior aligns with prior studies of undeformed rotating BTZ black holes [16,113], but the $T\bar{T}$ deformation introduces a critical threshold at μ_l , beyond which the theory becomes ill defined, describing the nonlocal nature of the deformation.

The butterfly velocity, however, exhibits a striking dependence on the $T\bar{T}$ deformation. For the nonrotating BTZ black hole, we find butterfly velocity as $v_B = \sqrt{1 - \frac{8\pi^2\mu}{\beta^2}}$, which is obtained consistently from shock wave analysis, pole skipping, and the entanglement wedge method. This result indicates a violation of the Mezei-Stanford bound, $v_B \leq 1$ for $d=2$, when the deformation parameter is negative ($\mu < 0$). It can be understood from the entanglement wedge method that the boundary region enclosing a falling particle propagates with the same v_B , which exceeds unity for negative μ . In the rotating case, the butterfly velocity in Schwarzschild coordinates further reveals a regime ($\mu_l < \mu < 0$) where v_B^+ exceeds the Mezei-Stanford bound, while at the Hagedorn bound ($\mu = \mu_{\text{Hagedorn}}$), v_B^+ reduces to the angular speed of the black hole. These violations seemingly suggest that the nonlocal effects of $T\bar{T}$ deformation allow chaos to propagate faster

than expected in two-derivative gravity. In the following, we provide some physical insights in support of such behavior:

- (i) Butterfly velocity and Lieb-Robinson bound: In local quantum lattice systems, the Lieb-Robinson (LR) bound establishes a strict, state-independent velocity v_{LR} that defines the fastest possible spread of information [120]. Roberts and Swingle argued that the butterfly velocity v_B , defined via the growth of out-of-time-order correlators (OTOCs), plays the role of a *state-dependent effective LR velocity* [121]. Unlike the universal microscopic LR velocity, v_B is sensitive to IR data such as temperature, charge density, and scaling exponents, thereby capturing the dynamical spread of chaos in a given state. This interpretation has been borne out both in free theories and strongly coupled holographic models [121]. $T\bar{T}$ -deformed theories are inherently nonlocal: the deformation couples the stress-tensor bilinear and effectively modifies the spacetime background on which the CFT resides [64,81]. In such cases, the assumptions underlying the standard LR bound (local Hamiltonian with finite-range interactions) no longer hold. Consequently, the butterfly velocity should not be constrained by the same universal light cone structure. Instead, it should be viewed as the natural *generalization* of the LR velocity in a nonlocal theory, i.e., a quantity that continues to bound the growth of commutators, but now with respect to the *effective causal structure* determined by the deformation. In other words, the superluminal v_B is consistent with the *nonlocal light cone* defined by the deformed theory, not with the original undeformed CFT light cone.
- (ii) Effect of attractive/repulsive interaction: As described in [64], for $\mu < 0$ a repulsive interparticle interaction leads to a time advance whenever (quasi) particles scatter off each other, causing an effective increase of the signal propagation speed. Physically, this corresponds to the deformation modifying the dispersion relation and rescaling the causal structure, so that excitations can propagate faster than in the undeformed CFT background. In the LR framework this would imply “superluminal” operator growth. However, because $T\bar{T}$ deformation modifies the background metric (equivalent to placing the theory on a curved spacetime slice), the physical interpretation is that the effective LR cone itself is rescaled.

We have provided a field theoretic analysis of the OTOC in Appendix A for the $T\bar{T}$ deformed theories following [52], where we find consistent result of the OTOC up to linear order in μ corroborating the holographic correspondence in the deformed setting. Additionally, we show that similar arguments hold from an analysis of the induced metric at the asymptotic boundary. Furthermore, our results are consistent with the cutoff prescription [64] discussed in Sec. V, wherein the boundary theory resides at a finite radial cutoff. The rescaled spatial coordinate in the cutoff

picture matches that of the mixed boundary condition approach, ensuring that chaos parameters computed in both frameworks are consistent. This equivalence strengthens the holographic interpretation of $T\bar{T}$ deformation as a geometric modification of the bulk, either via a finite cutoff or mixed boundary conditions at the asymptotic boundary [64,81]. In Appendix B, we investigate the late time behavior of the mutual information for the case of spherical shock in the deformed nonrotating BTZ geometry and obtained the scrambling time, which exhibits nontrivial dependence on the deformation parameter μ .

For future directions, it would be interesting to explore the implications of our results for other holographic probes, such as complexity, in $T\bar{T}$ deformed theories. A crucial outstanding issue in this context would be a nonperturbative analysis of the Krylov complexity [122–124] in $T\bar{T}$ -deformed AdS_3 geometries utilizing the holographic autocorrelation function as well as the momentum-Krylov complexity correspondence [125], extending the perturbative analysis in [126]. The behavior of the butterfly velocity near the Hagedorn bound requires further investigation, particularly in relation to the stability of the deformed CFT_2 .

ACKNOWLEDGMENTS

The authors are supported by the NSFC Grant No. 12447108 and the Shing-Tung Yau Center of Southeast University. The authors are grateful to Yunfeng Jiang, Suchetan Das, Vinay Malvimat, Mingshuai Xu, and Juan Pedraza for useful suggestions and comments on the draft.

DATA AVAILABILITY

No data were created or analyzed in this study.

APPENDIX A: OTOC IN $T\bar{T}$ DEFORMED CFT_2

1. Conformal perturbation theory

In this appendix, we investigate the OTOC between pairs of operators in the $T\bar{T}$ deformed CFT_2 at a finite temperature, defined on a cylinder \mathcal{M} with circumference β ,

$$\frac{\langle W(t)VW(t)V \rangle_\beta}{\langle W(t)W(t) \rangle_\beta \langle VV \rangle_\beta} \quad (A1)$$

in order to investigate the chaotic properties perturbatively. These computations mostly follow [52] and are included to make the manuscript self-contained. Note that the action functional for the $T\bar{T}$ deformed CFT_2 in Eq. (2.1) may be expanded for a small deformation parameter μ as follows

$$\mathcal{S}^{[\mu]} = \mathcal{S}_{\text{CFT}} - \frac{\mu}{\pi^2} \int_{\mathcal{M}} d^2x T\bar{T}, \quad (A2)$$

where we have assumed a flat background metric $\gamma_{ab}dx^a dx^b = dwd\bar{w}$, and denoted¹⁴

$$T := 2\pi T_{ww}, \quad \bar{T} := 2\pi T_{\bar{w}\bar{w}}. \quad (A3)$$

According to (A2), any correlation function in the deformed theory may be computed perturbatively as follows

$$\begin{aligned} \langle \mathcal{O}_1(w_1, \bar{w}_1) \cdots \rangle^{[\mu]} &= \int \mathcal{D}\phi(\mathcal{O}_1(w_1, \bar{w}_1) \cdots) e^{-\mathcal{S}^{[\mu]}[\phi]} \\ &= \int \mathcal{D}\phi(\mathcal{O}_1(w_1, \bar{w}_1) \cdots) e^{-\mathcal{S}_{\text{CFT}} + \frac{\mu}{\pi^2} \int_{\mathcal{M}} d^2x T\bar{T}} \\ &\approx \int \mathcal{D}\phi(\mathcal{O}_1(w_1, \bar{w}_1) \cdots) e^{-\mathcal{S}_{\text{CFT}}} \left(1 + \frac{\mu}{\pi^2} \int_{\mathcal{M}} d^2x T\bar{T} \mathcal{O}(\mu^2) \right) \\ &= \langle \mathcal{O}_1(w_1, \bar{w}_1) \cdots \rangle^{[0]} + \frac{\mu}{\pi^2} \int d^2x \langle T(w)\bar{T}(\bar{w}) \mathcal{O}_1(w_1, \bar{w}_1) \cdots \rangle^{[0]} + \mathcal{O}(\mu^2) \end{aligned} \quad (A4)$$

where ϕ collectively denotes the field content of the CFT and the superscripts on the correlators denote whether they are evaluated in the (un)deformed theory. Now the leading correction to the four-point OTOC in Eq. (A1) may be obtained as follows

$$\begin{aligned} &\frac{\langle W(w_1, \bar{w}_1)W(w_2, \bar{w}_2)V(w_3, \bar{w}_3)V(w_4, \bar{w}_4) \rangle_\beta}{\langle W(w_1, \bar{w}_1)W(w_2, \bar{w}_2) \rangle_\beta \langle V(w_3, \bar{w}_3)V(w_4, \bar{w}_4) \rangle_\beta} \left(1 + \frac{\mu}{\pi^2} \int_{\mathcal{M}} d^2x \frac{\langle T(w)\bar{T}(\bar{w})W(w_1, \bar{w}_1)W(w_2, \bar{w}_2)V(w_3, \bar{w}_3)V(w_4, \bar{w}_4) \rangle_\beta}{\langle W(w_1, \bar{w}_1)W(w_2, \bar{w}_2)V(w_3, \bar{w}_3)V(w_4, \bar{w}_4) \rangle_\beta} \right. \\ &\quad \left. - \frac{\mu}{\pi^2} \int_{\mathcal{M}} d^2x \frac{\langle T(w)\bar{T}(\bar{w})W(w_1, \bar{w}_1)W(w_2, \bar{w}_2) \rangle_\beta}{\langle W(w_1, \bar{w}_1)W(w_2, \bar{w}_2) \rangle_\beta} - \frac{\mu}{\pi^2} \int_{\mathcal{M}} d^2x \frac{\langle T(w)\bar{T}(\bar{w})V(w_3, \bar{w}_3)V(w_4, \bar{w}_4) \rangle_\beta}{\langle V(w_3, \bar{w}_3)V(w_4, \bar{w}_4) \rangle_\beta} \right) \end{aligned} \quad (A5)$$

¹⁴Note that the trace $T_{w\bar{w}}$ has been dropped assuming that the seed theory is a CFT.

where we have dropped the superscripts for brevity. We map the desired correlators onto the complex plane \mathbb{C} using the conformal transformations

$$z = e^{\frac{2\pi w}{\beta}}, \quad \bar{z} = e^{\frac{2\pi \bar{w}}{\beta}}. \quad (\text{A6})$$

Under this transformation, the stress tensor components transform as follows

$$T(w) = \left(\frac{2\pi z}{\beta}\right)^2 T(z) - \frac{\pi^2 c}{6\beta^2}, \quad \bar{T}(w) = \left(\frac{2\pi \bar{z}}{\beta}\right)^2 \bar{T}(z) - \frac{\pi^2 c}{6\beta^2}, \quad (\text{A7})$$

where c is the central charge of the undeformed CFT_2 . Now the correlation functions with stress tensor insertions may be computed using the conformal Ward identities as follows [117,127,128]:

$$\begin{aligned} & \frac{\langle T(w)\bar{T}(w)W(w_1, \bar{w}_1)W(w_2, \bar{w}_2)V(w_3, \bar{w}_3)V(w_4, \bar{w}_4) \rangle_\beta}{\langle W(w_1, \bar{w}_1)W(w_2, \bar{w}_2)V(w_3, \bar{w}_3)V(w_4, \bar{w}_4) \rangle_\beta} \\ &= \frac{1}{\langle W(w_1, \bar{w}_1)W(w_2, \bar{w}_2)V(w_3, \bar{w}_3)V(w_4, \bar{w}_4) \rangle_\mathbb{C}} \left[-\frac{\pi^2 c}{6\beta^2} + \left(\frac{2\pi z}{\beta}\right)^2 \sum_{j=1}^4 \left(\frac{h_j}{(z-z_j)^2} + \frac{1}{z-z_j} \partial_j \right) \right] \\ & \times \left[-\frac{\pi^2 c}{6\beta^2} + \left(\frac{2\pi \bar{z}}{\beta}\right)^2 \sum_{j=1}^4 \left(\frac{\bar{h}_j}{(\bar{z}-\bar{z}_j)^2} + \frac{1}{\bar{z}-\bar{z}_j} \bar{\partial}_j \right) \right] \langle W(w_1, \bar{w}_1)W(w_2, \bar{w}_2)V(w_3, \bar{w}_3)V(w_4, \bar{w}_4) \rangle_\mathbb{C}. \end{aligned} \quad (\text{A8})$$

The four-point function on the complex plane may be expanded in terms of conformal blocks, and in the large central charge limit with $\frac{h_w}{c}$ fixed and $1 \ll h_w \ll c$, the dominant contribution comes from the vacuum block given by [2]

$$\mathcal{F}_0(\eta) = \left(\frac{\eta}{1 - (1-\eta)^{1-12h_w/c}} \right)^{2h_w}, \quad \eta = \frac{z_{12}z_{34}}{z_{13}z_{24}}. \quad (\text{A9})$$

Near $\eta \sim 0$, the block simplifies to

$$\mathcal{F}_0(\eta) \approx \left(\frac{1}{1 - \frac{24\pi i h_w}{c\eta}} \right)^{2h_w}, \quad \bar{\mathcal{F}}_0(\bar{\eta}) \sim 1. \quad (\text{A10})$$

The left-hand side of (A8) becomes

$$\begin{aligned} & \left(-\frac{\pi^2 c}{6\beta^2} \right)^2 - \frac{\pi^2 c}{6\beta^2} \left(\frac{2\pi \bar{z}}{\beta} \right)^2 \sum_{j=1}^4 \frac{\bar{h}_j}{(\bar{z}-\bar{z}_j)^2} - \frac{\pi^2 c}{6\beta^2} \left(\frac{2\pi z}{\beta} \right)^2 \sum_{j=1}^4 \left(\frac{h_j}{(z-z_j)^2} + \frac{\partial_j \log \mathcal{F}_0(\eta)}{z-z_j} \right) \\ & + \left(\frac{2\pi z}{\beta} \right)^2 \left(\frac{2\pi \bar{z}}{\beta} \right)^2 \sum_{i=1}^4 \left(\frac{h_i}{(z-z_i)^2} + \frac{\partial_i \log \mathcal{F}_0(\eta)}{z-z_i} \right) \sum_{j=1}^4 \frac{\bar{h}_j}{(\bar{z}-\bar{z}_j)^2}. \end{aligned} \quad (\text{A11})$$

Following [3,31], to compute the leading correction to the OTOC, we now place the operators as

$$\begin{aligned} z_1 &= e^{\frac{2\pi i \epsilon_1}{\beta}}, & \bar{z}_1 &= e^{-\frac{2\pi i \epsilon_1}{\beta}}, \\ z_2 &= e^{\frac{2\pi i \epsilon_2}{\beta}}, & \bar{z}_2 &= e^{-\frac{2\pi i \epsilon_2}{\beta}}, \\ z_3 &= e^{\frac{2\pi i(t-x+i\epsilon_3)}{\beta}}, & \bar{z}_3 &= e^{\frac{2\pi i(-t-x-i\epsilon_3)}{\beta}}, \\ z_4 &= e^{\frac{2\pi i(t-x+i\epsilon_4)}{\beta}}, & \bar{z}_4 &= e^{\frac{2\pi i(-t-x-i\epsilon_4)}{\beta}}, \end{aligned} \quad (\text{A12})$$

where without loss of generality, we may choose [31]

$$\epsilon_2 = \epsilon_1 + \frac{\beta}{2}, \quad \epsilon_4 = \epsilon_3 + \frac{\beta}{2}, \quad \epsilon_1 = 0. \quad (\text{A13})$$

Upon simplifying (A11), adding the contributions from the two-point functions in Eq. (A5) and subsequently performing the integrals utilizing the method elaborated in [116,117], we may obtain the OTOC as follows

$$\frac{\langle W(t)VW(t)V \rangle_\beta}{\langle W(t)W(t) \rangle_\beta \langle VV \rangle_\beta} \left(1 + \mu f_1(x) + \mu f_2(x) e^{-\frac{2\pi t}{\beta}} + \dots \right) \quad (\text{A14})$$

where $f_{1,2}(x)$ are complicated functions of x . Note that, similar to [52], we have neglected a nondynamical divergent piece originating from the integral of the constant term in Eq. (A11) which only depends on the cutoff. In the above expression, the leading late time behavior is still governed by the factor $e^{\frac{2\pi t}{\beta}}$ and hence the Lyapunov exponent is undeformed. One may also perform similar computations in the presence of a finite angular momentum utilizing the techniques in [114] to map the twisted cylinder with periodic identifications on both directions into the thermal cylinder with only a temporal identification.

2. From induced metric at the asymptotic boundary

Alternatively, we may perform the computations of OTOC in the dual field theory by noting that the induced metric on the asymptotic boundary of (3.2) is given by

$$\begin{aligned} ds_{\text{bdy}}^2 &= -\frac{dt^2}{(1+2\mu\mathcal{L}_\mu)^2} + \frac{dx^2}{(1-2\mu\mathcal{L}_\mu)^2} \\ &\equiv \frac{1}{(1+2\mu\mathcal{L}_\mu)^2} (-dt^2 + d\hat{x}^2), \end{aligned} \quad (\text{A15})$$

which is conformally flat with the rescaled spatial coordinate

$$\hat{x} = \frac{1+2\mu\mathcal{L}_\mu}{1-2\mu\mathcal{L}_\mu} x. \quad (\text{A16})$$

Therefore, the undeformed result for the OTOC computed in [3] is easily translated to the deformed case as follows¹⁵

$$\begin{aligned} \frac{\langle W(t)VW(t)V \rangle_\beta}{\langle W(t)W(t) \rangle_\beta \langle VV \rangle_\beta} &\approx \left[\frac{1}{1 + \frac{24\pi i h_w}{\epsilon_{12}^* \epsilon_{34}} e^{\frac{2\pi}{\beta}(t-t_*-\hat{x})}} \right]^{2h_v} \\ &= \left[1 + \frac{24\pi i h_w}{\epsilon_{12}^* \epsilon_{34}} e^{\frac{2\pi}{\beta} \left(t-t_* - \frac{x}{\sqrt{1-\frac{8\pi^2\mu}{\beta^2}}} \right)} \right]^{-2h_v} \end{aligned} \quad (\text{A17})$$

¹⁵We follow the conventions in [3]. Note that the conformal factors get canceled in the numerator and denominator.

where we have utilized Eq. (3.3). Remarkably, the above expression correctly reproduces both the Lyapunov exponent and the butterfly velocity as obtained from the bulk computations. In the presence of a finite chemical potential, a similar analysis of the induced metric on the asymptotic boundary of (4.7), it is possible to reproduce our results following the analysis in [112].

APPENDIX B: MUTUAL INFORMATION

In this appendix, we investigate the late time behavior of the mutual information between two subsystems in the shock wave geometries corresponding to $\text{T}\bar{\text{T}}$ deformed AdS_3 . For simplicity, we restrict our analysis to the spherical shock in the deformed nonrotating BTZ black hole (3.2). Consider two equal size subsystems $A = [-\frac{\ell}{2}, \frac{\ell}{2}]$ at $t_L = 0$ on the left asymptotic boundary and $B = [-\frac{\ell}{2}, \frac{\ell}{2}]$ at $t_R = 0$ on the right asymptotic boundary. The mutual information between regions A and B is expressed as,

$$I(A:B) = S_A + S_B - S_{AB}, \quad (\text{B1})$$

where the entanglement entropies of subsystems A and B are given by the well-known result independent of the shock wave [7]

$$\begin{aligned} S_A = S_B &= \frac{1}{2G_N} \log \left[\frac{r_\infty}{\sqrt{L}} \sinh \frac{\sqrt{\mathcal{L}_\mu} \ell}{1-2\mu\mathcal{L}_\mu} \right], \\ &= \frac{1}{2G_N} \log \left[\frac{\beta - \sqrt{\beta^2 - 8\pi^2\mu}}{4\pi\mu\epsilon_c} \sinh \frac{\pi\ell}{\sqrt{\beta^2 - 8\pi^2\mu}} \right], \end{aligned} \quad (\text{B2})$$

and from Eq. (3.28),

$$S_{AB} = 2 \times \frac{1}{2G_N} \log \left[\frac{r_\infty}{\sqrt{L}} \left(1 + \frac{\alpha}{2} \right) \right]. \quad (\text{B3})$$

For a large black hole ($M \gg 1$), one obtains the mutual information to be

$$\begin{aligned} I(A:B) &\sim \frac{1}{G_N} \left[\log \sinh \frac{\pi\ell}{\sqrt{\beta^2 - 8\pi^2\mu}} - \lambda_L t_w \right. \\ &\quad \left. - \log \left(\frac{E}{8M} \frac{1+2\mu\mathcal{L}_\mu}{1-2\mu\mathcal{L}_\mu} \right) \right]. \end{aligned} \quad (\text{B4})$$

Scrambling time: The scrambling time is defined as the timescale at which the mutual information vanishes, $I(A:B) = 0$. In our case, the scrambling time may be obtained from Eq. (B4) as follows

$$\begin{aligned} t_* &= \frac{\beta}{2\pi} \log \left[\frac{8M}{E} \sqrt{1 - \frac{8\pi^2\mu}{\beta^2}} \sinh \frac{\pi\ell}{\sqrt{\beta^2 - 8\pi^2\mu}} \right], \\ &\sim \frac{\ell}{2\sqrt{\beta^2 - 8\pi^2\mu}} + \frac{\beta}{2\pi} \log \left[\frac{8M}{E} \sqrt{1 - \frac{8\pi^2\mu}{\beta^2}} \right]. \end{aligned} \quad (\text{B5})$$

- [1] F. A. Dolan and H. Osborn, Conformal four point functions and the operator product expansion, *Nucl. Phys.* **B599**, 459 (2001).
- [2] A. L. Fitzpatrick, J. Kaplan, and M. T. Walters, Universality of long-distance AdS physics from the CFT bootstrap, *J. High Energy Phys.* **08** (2014) 145.
- [3] D. A. Roberts and D. Stanford, Two-dimensional conformal field theory and the butterfly effect, *Phys. Rev. Lett.* **115**, 131603 (2015).
- [4] S. Grozdanov, K. Schalm, and V. Scopelliti, Black hole scrambling from hydrodynamics, *Phys. Rev. Lett.* **120**, 231601 (2018).
- [5] M. Mezei and D. Stanford, On entanglement spreading in chaotic systems, *J. High Energy Phys.* **05** (2017) 065.
- [6] Y. Sekino and L. Susskind, Fast scramblers, *J. High Energy Phys.* **10** (2008) 065.
- [7] S. H. Shenker and D. Stanford, Black holes and the butterfly effect, *J. High Energy Phys.* **03** (2014) 067.
- [8] J. M. Maldacena, The large N limit of superconformal field theories and supergravity, *Adv. Theor. Math. Phys.* **2**, 231 (1998).
- [9] S. S. Gubser, I. R. Klebanov, and A. M. Polyakov, Gauge theory correlators from noncritical string theory, *Phys. Lett. B* **428**, 105 (1998).
- [10] S. Xu and B. Swingle, Locality, quantum fluctuations, and scrambling, *Phys. Rev. X* **9**, 031048 (2019).
- [11] H. Gharibyan, M. Hanada, B. Swingle, and M. Tezuka, Quantum Lyapunov spectrum, *J. High Energy Phys.* **04** (2019) 082.
- [12] J. Steinberg and B. Swingle, Thermalization and chaos in QED₃, *Phys. Rev. D* **99**, 076007 (2019).
- [13] Y. Gu, A. Kitaev, and P. Zhang, A two-way approach to out-of-time-order correlators, *J. High Energy Phys.* **03** (2022) 133.
- [14] R. R. Poojary, BTZ dynamics and chaos, *J. High Energy Phys.* **03** (2020) 048.
- [15] A. Banerjee, A. Kundu, and R. R. Poojary, Strings, branes, Schwarzian action and maximal chaos, *Phys. Lett. B* **838**, 137632 (2023).
- [16] V. Malvimat and R. R. Poojary, Fast scrambling due to rotating shockwaves in BTZ, *Phys. Rev. D* **105**, 126019 (2022).
- [17] S. Das, B. Ezhuthachan, A. Kundu, S. Porey, B. Roy, and K. Sengupta, Out-of-time-order correlators in driven conformal field theories, *J. High Energy Phys.* **08** (2022) 221.
- [18] S. Das, B. Ezhuthachan, A. Kundu, S. Porey, and B. Roy, Critical quenches, OTOCs and early-time chaos, *J. High Energy Phys.* **07** (2022) 046.
- [19] S. Das, B. Ezhuthachan, and A. Kundu, Real time dynamics from low point correlators in 2d BCFT, *J. High Energy Phys.* **12** (2019) 141.
- [20] R. Fan, P. Zhang, H. Shen, and H. Zhai, Out-of-time-order correlation for many-body localization, *Sci. Bull.* **62**, 707 (2017).
- [21] P. Biswas, B. Ezhuthachan, A. Kundu, and B. Roy, Moving mirrors, OTOCs and scrambling, *J. High Energy Phys.* **10** (2024) 146.
- [22] B. Baishya, A. Chakraborty, and N. Padhi, A study of three butterflies: Entanglement wedge method, OTOC and pole-skipping, *Phys. Rev. D* **111**, 106013 (2025).
- [23] A. Banerjee, A. Bhattacharyya, P. Drashni, and S. Pawar, From CFTs to theories with Bondi-Metzner-Sachs symmetries: Complexity and out-of-time-ordered correlators, *Phys. Rev. D* **106**, 126022 (2022).
- [24] V. Balasubramanian, B. Craps, M. De Clerck, and K. Nguyen, Superluminal chaos after a quantum quench, *J. High Energy Phys.* **12** (2019) 132.
- [25] B. Craps, M. De Clerck, P. Hacker, K. Nguyen, and C. Rabideau, Slow scrambling in extremal BTZ and microstate geometries, *J. High Energy Phys.* **03** (2021) 020.
- [26] S. Chakraborty, H. Hoshino, S. Pant, and K. Sil, A holographic study of the characteristics of chaos and correlation in the presence of backreaction, *Phys. Lett. B* **838**, 137749 (2023).
- [27] S. Xu and B. Swingle, Scrambling dynamics and out-of-time-ordered correlators in quantum many-body systems, *PRX Quantum* **5**, 010201 (2024).
- [28] S. Das, B. Ezhuthachan, A. Kundu, S. Porey, B. Roy, and K. Sengupta, Brane detectors of a dynamical phase transition in a driven CFT, *SciPost Phys.* **15**, 202 (2023).
- [29] K. Hashimoto, K.-B. Huh, K.-Y. Kim, and R. Watanabe, Exponential growth of out-of-time-order correlator without chaos: Inverted harmonic oscillator, *J. High Energy Phys.* **11** (2020) 068.
- [30] S. Khetrpal, Chaos and operator growth in 2d CFT, *J. High Energy Phys.* **03** (2023) 176.
- [31] E. Perlmutter, Bounding the space of holographic CFTs with chaos, *J. High Energy Phys.* **10** (2016) 069.
- [32] A. Saha and S. Gangopadhyay, Quantum chaos in the presence of nonconformality, *Phys. Rev. D* **110**, 026025 (2024).
- [33] D. A. Roberts, D. Stanford, and L. Susskind, Localized shocks, *J. High Energy Phys.* **03** (2015) 051.
- [34] S. Ryu and T. Takayanagi, Holographic derivation of entanglement entropy from AdS/CFT, *Phys. Rev. Lett.* **96**, 181602 (2006).
- [35] S. Ryu and T. Takayanagi, Aspects of holographic entanglement entropy, *J. High Energy Phys.* **08** (2006) 045.
- [36] V. E. Hubeny, M. Rangamani, and T. Takayanagi, A covariant holographic entanglement entropy proposal, *J. High Energy Phys.* **07** (2007) 062.
- [37] J. Maldacena, S. H. Shenker, and D. Stanford, A bound on chaos, *J. High Energy Phys.* **08** (2016) 106.
- [38] M. Mezei, On entanglement spreading from holography, *J. High Energy Phys.* **05** (2017) 064.
- [39] M. Blake, R. A. Davison, S. Grozdanov, and H. Liu, Many-body chaos and energy dynamics in holography, *J. High Energy Phys.* **10** (2018) 035.
- [40] M. Blake, H. Lee, and H. Liu, A quantum hydrodynamical description for scrambling and many-body chaos, *J. High Energy Phys.* **10** (2018) 127.
- [41] S. Grozdanov, On the connection between hydrodynamics and quantum chaos in holographic theories with stringy corrections, *J. High Energy Phys.* **01** (2019) 048.
- [42] M. Blake, R. A. Davison, and D. Vegh, Horizon constraints on holographic Green's functions, *J. High Energy Phys.* **01** (2020) 077.
- [43] D. Wang and Z.-Y. Wang, Pole skipping in holographic theories with bosonic fields, *Phys. Rev. Lett.* **129**, 231603 (2022).

- [44] S. Ning, D. Wang, and Z.-Y. Wang, Pole skipping in holographic theories with gauge and fermionic fields, *J. High Energy Phys.* **12** (2023) 084.
- [45] J. Cardy, The $T\bar{T}$ deformation of quantum field theory as random geometry, *J. High Energy Phys.* **10** (2018) 186.
- [46] S. Dubovsky, V. Gorbenko, and G. Hernández-Chifflet, $T\bar{T}$ partition function from topological gravity, *J. High Energy Phys.* **09** (2018) 158.
- [47] S. Datta and Y. Jiang, $T\bar{T}$ deformed partition functions, *J. High Energy Phys.* **08** (2018) 106.
- [48] O. Aharony, S. Datta, A. Giveon, Y. Jiang, and D. Kutasov, Modular invariance and uniqueness of $T\bar{T}$ deformed CFT, *J. High Energy Phys.* **01** (2019) 086.
- [49] A. B. Zamolodchikov, Expectation value of composite field T anti- T in two-dimensional quantum field theory, [arXiv:hep-th/0401146](https://arxiv.org/abs/hep-th/0401146).
- [50] A. Cavaglià, S. Negro, I. M. Szécsényi, and R. Tateo, $T\bar{T}$ -deformed 2D quantum field theories, *J. High Energy Phys.* **10** (2016) 112.
- [51] F. A. Smirnov and A. B. Zamolodchikov, On space of integrable quantum field theories, *Nucl. Phys.* **B915**, 363 (2017).
- [52] S. He and H. Shu, Correlation functions, entanglement and chaos in the $T\bar{T}/J\bar{T}$ -deformed CFTs, *J. High Energy Phys.* **02** (2020) 088.
- [53] S. He, Y. Sun, and Y.-X. Zhang, $T\bar{T}$ -flow effects on torus partition functions, *J. High Energy Phys.* **09** (2021) 061.
- [54] S. He, P. H. C. Lau, Z.-Y. Xian, and L. Zhao, Quantum chaos, scrambling and operator growth in $T\bar{T}$ deformed SYK models, *J. High Energy Phys.* **12** (2022) 070.
- [55] S. He, J. Yang, Y.-X. Zhang, and Z.-X. Zhao, Pseudo entropy of primary operators in $T\bar{T}/J\bar{T}$ -deformed CFTs, *J. High Energy Phys.* **09** (2023) 025.
- [56] J. Tian, On-shell action of $T\bar{T}$ -deformed Holographic CFTs, [arXiv:2306.01258](https://arxiv.org/abs/2306.01258).
- [57] J. Tian, T. Lai, and F. Omid, Modular transformations of on-shell actions of (root-) $T\bar{T}$ deformed holographic CFTs, *Nucl. Phys.* **B1007**, 116675 (2024).
- [58] M. He, J. Hou, and Y. Jiang, $T\bar{T}$ -deformed entanglement entropy for IQFT, *J. High Energy Phys.* **03** (2024) 056.
- [59] M. He and Y. Sun, Holographic entanglement entropy in $T\bar{T}$ -deformed AdS₃, *Nucl. Phys.* **B990**, 116190 (2023).
- [60] M. He, One-loop partition functions in $T\bar{T}$ -deformed AdS₃, *J. High Energy Phys.* **05** (2024) 067.
- [61] S. Dubovsky, V. Gorbenko, and M. Mirbabayi, Asymptotic fragility, near AdS₂ holography and $T\bar{T}$, *J. High Energy Phys.* **09** (2017) 136.
- [62] N. Callebaut, J. Kruthoff, and H. Verlinde, $T\bar{T}$ deformed CFT as a non-critical string, *J. High Energy Phys.* **04** (2020) 084.
- [63] A. J. Tolley, $T\bar{T}$ deformations, massive gravity and non-critical strings, *J. High Energy Phys.* **06** (2020) 050.
- [64] L. McGough, M. Mezei, and H. Verlinde, Moving the CFT into the bulk with $T\bar{T}$, *J. High Energy Phys.* **04** (2018) 010.
- [65] P. Kraus, J. Liu, and D. Marolf, Cutoff AdS₃ versus the $T\bar{T}$ deformation, *J. High Energy Phys.* **07** (2018) 027.
- [66] M. Taylor, $T\bar{T}$ deformations in general dimensions, *Adv. Theor. Math. Phys.* **27**, 37 (2023).
- [67] P. Kraus, R. Monten, and K. Roumpedakis, Refining the cutoff 3d gravity/ $T\bar{T}$ correspondence, *J. High Energy Phys.* **10** (2022) 094.
- [68] M. Asrat, A. Giveon, N. Itzhaki, and D. Kutasov, Holography beyond AdS, *Nucl. Phys.* **B932**, 241 (2018).
- [69] V. Shyam, Background independent holographic dual to $T\bar{T}$ deformed CFT with large central charge in 2 dimensions, *J. High Energy Phys.* **10** (2017) 108.
- [70] W. Cottrell and A. Hashimoto, Comments on $T\bar{T}$ double trace deformations and boundary conditions, *Phys. Lett. B* **789**, 251 (2019).
- [71] T. Hartman, J. Kruthoff, E. Shaghoulian, and A. Tajdini, Holography at finite cutoff with a T^2 deformation, *J. High Energy Phys.* **03** (2019) 004.
- [72] V. Shyam, Finite cutoff AdS₅ holography and the generalized gradient flow, *J. High Energy Phys.* **12** (2018) 086.
- [73] G. Jafari, A. Naseh, and H. Zolfi, Path integral optimization for $T\bar{T}$ deformation, *Phys. Rev. D* **101**, 026007 (2020).
- [74] P. Caputa, S. Datta, and V. Shyam, Sphere partition functions & cut-off AdS, *J. High Energy Phys.* **05** (2019) 112.
- [75] A. Lewkowycz, J. Liu, E. Silverstein, and G. Torroba, $T\bar{T}$ and EE, with implications for (A)dS subregion encodings, *J. High Energy Phys.* **04** (2020) 152.
- [76] A. Giveon, N. Itzhaki, and D. Kutasov, A solvable irrelevant deformation of AdS₃/CFT₂, *J. High Energy Phys.* **12** (2017) 155.
- [77] J.-C. Chang, S. He, Y.-X. Liu, and L. Zhao, The holographic $T\bar{T}$ deformation of the entanglement entropy in (A)dS₃/CFT₂, *Phys. Rev. D* **112**, 026013 (2025).
- [78] S. Pant and H. Parihar, Mixed state entanglement in deformed field theory at finite temperature, *Phys. Rev. D* **111**, 086020 (2025).
- [79] L. Apolo, P.-X. Hao, W.-X. Lai, and W. Song, Glue-on AdS holography for $T\bar{T}$ -deformed CFTs, *J. High Energy Phys.* **06** (2023) 117.
- [80] L. Apolo, P.-X. Hao, W.-X. Lai, and W. Song, Extremal surfaces in glue-on AdS/ $T\bar{T}$ holography, *J. High Energy Phys.* **01** (2024) 054.
- [81] M. Guica and R. Monten, $T\bar{T}$ and the mirage of a bulk cutoff, *SciPost Phys.* **10**, 024 (2021).
- [82] S. Hirano and M. Shigemori, Random boundary geometry and gravity dual of $T\bar{T}$ deformation, *J. High Energy Phys.* **11** (2020) 108.
- [83] S. Hirano, T. Nakajima, and M. Shigemori, $T\bar{T}$ Deformation of stress-tensor correlators from random geometry, *J. High Energy Phys.* **04** (2021) 270.
- [84] T. Faulkner, H. Liu, and M. Rangamani, Integrating out geometry: Holographic Wilsonian RG and the membrane paradigm, *J. High Energy Phys.* **08** (2011) 051.
- [85] I. Heemskerck and J. Polchinski, Holographic and Wilsonian renormalization groups, *J. High Energy Phys.* **06** (2011) 031.
- [86] V. Balasubramanian, M. Guica, and A. Lawrence, Holographic interpretations of the renormalization group, *J. High Energy Phys.* **01** (2013) 115.
- [87] Y. Jiang, A pedagogical review on solvable irrelevant deformations of 2D quantum field theory, *Commun. Theor. Phys.* **73**, 057201 (2021).

- [88] S. He, Y. Li, H. Ouyang, and Y. Sun, $T\bar{T}$ deformation: Introduction and some recent advances, *Sci. China Phys. Mech. Astron.* **68**, 101001 (2025).
- [89] K. Skenderis and S. N. Solodukhin, Quantum effective action from the AdS/CFT correspondence, *Phys. Lett. B* **472**, 316 (2000).
- [90] M. Banados, Three-dimensional quantum geometry and black holes, *AIP Conf. Proc.* **484** (1999) 147.
- [91] A. Banerjee and P. Roy, Bounds on $T\bar{T}$ deformation from entanglement, *J. High Energy Phys.* **10** (2024) 064.
- [92] J. M. Maldacena, Eternal black holes in anti-de Sitter, *J. High Energy Phys.* **04** (2003) 021.
- [93] T. Hartman and J. Maldacena, Time evolution of entanglement entropy from black hole interiors, *J. High Energy Phys.* **05** (2013) 014.
- [94] T. Dray and G. 't Hooft, The gravitational shock wave of a massless particle, *Nucl. Phys.* **B253**, 173 (1985).
- [95] T. Dray and G. 't Hooft, The effect of spherical shells of matter on the schwarzschild Black Hole, *Commun. Math. Phys.* **99**, 613 (1985).
- [96] M. Hotta and M. Tanaka, Shock wave geometry with nonvanishing cosmological constant, *Classical Quantum Gravity* **10**, 307 (1993).
- [97] K. Sfetsos, On gravitational shock waves in curved spacetimes, *Nucl. Phys.* **B436**, 721 (1995).
- [98] R.-G. Cai and J. B. Griffiths, Null particle solutions in three-dimensional (anti-)de Sitter spaces, *J. Math. Phys.* **40**, 3465 (1999).
- [99] L. Cornalba, M. S. Costa, J. Penedones, and R. Schiappa, Eikonal approximation in AdS/CFT: From shock waves to four-point functions, *J. High Energy Phys.* **08** (2007) 019.
- [100] S. H. Shenker and D. Stanford, Stringy effects in scrambling, *J. High Energy Phys.* **05** (2015) 132.
- [101] X.-L. Qi and Z. Yang, Butterfly velocity and bulk causal structure, [arXiv:1705.01728](https://arxiv.org/abs/1705.01728).
- [102] W. Fischler, V. Jahnke, and J. F. Pedraza, Chaos and entanglement spreading in a non-commutative gauge theory, *J. High Energy Phys.* **11** (2018) 072.
- [103] S. Eccles, W. Fischler, T. Guglielmo, J. F. Pedraza, and S. Racz, Speeding up the spread of quantum information in chaotic systems, *J. High Energy Phys.* **12** (2021) 019.
- [104] D. Giataganas, U. Gürsoy, and J. F. Pedraza, Strongly-coupled anisotropic gauge theories and holography, *Phys. Rev. Lett.* **121**, 121601 (2018).
- [105] U. Gürsoy, M. Järvinen, G. Nijs, and J. F. Pedraza, On the interplay between magnetic field and anisotropy in holographic QCD, *J. High Energy Phys.* **03** (2021) 180.
- [106] S. Dubovsky, R. Flauger, and V. Gorbenko, Solving the simplest theory of quantum gravity, *J. High Energy Phys.* **09** (2012) 133.
- [107] Y. Liu and A. Raju, Quantum chaos in topologically massive gravity, *J. High Energy Phys.* **12** (2020) 027.
- [108] N. Ceplak and D. Vegh, Pole-skipping and Rarita-Schwinger fields, *Phys. Rev. D* **103**, 106009 (2021).
- [109] X. Dong, D. Wang, W. W. Weng, and C.-H. Wu, A tale of two butterflies: An exact equivalence in higher-derivative gravity, *J. High Energy Phys.* **10** (2022) 009.
- [110] V. Malvimat and R. R. Poojary, Fast scrambling of mutual information in Kerr-AdS₅, *J. High Energy Phys.* **03** (2023) 099.
- [111] V. Malvimat and R. R. Poojary, Fast scrambling of mutual information in Kerr-AdS₄ spacetime, *Phys. Rev. D* **107**, 026019 (2023).
- [112] B. Craps, S. Khetrapal, and C. Rabideau, Chaos in CFT dual to rotating BTZ, *J. High Energy Phys.* **11** (2021) 105.
- [113] V. Jahnke, K.-Y. Kim, and J. Yoon, On the chaos bound in rotating black holes, *J. High Energy Phys.* **05** (2019) 037.
- [114] D. Basu and S. Biswas, Entanglement, $T\bar{T}$ and rotating black holes, *J. High Energy Phys.* **03** (2025) 167.
- [115] M. Mezei and G. Sárosi, Chaos in the butterfly cone, *J. High Energy Phys.* **01** (2020) 186.
- [116] B. Chen, L. Chen, and P.-X. Hao, Entanglement entropy in $T\bar{T}$ -deformed CFT, *Phys. Rev. D* **98**, 086025 (2018).
- [117] H.-S. Jeong, K.-Y. Kim, and M. Nishida, Entanglement and Rényi entropy of multiple intervals in $T\bar{T}$ -deformed CFT and holography, *Phys. Rev. D* **100**, 106015 (2019).
- [118] W. Z. Chua, T. Hartman, and W. W. Weng, Replica manifolds, pole skipping, and the butterfly effect, [arXiv:2504.08139](https://arxiv.org/abs/2504.08139).
- [119] C. Murdia, Y. Nomura, P. Rath, and N. Salzetta, Comments on holographic entanglement entropy in TT deformed conformal field theories, *Phys. Rev. D* **100**, 026011 (2019).
- [120] E. H. Lieb and D. W. Robinson, The finite group velocity of quantum spin systems, *Commun. Math. Phys.* **28**, 251 (1972).
- [121] D. A. Roberts and B. Swingle, Lieb-Robinson bound and the butterfly effect in quantum field theories, *Phys. Rev. Lett.* **117**, 091602 (2016).
- [122] D. E. Parker, X. Cao, A. Avdoshkin, T. Scaffidi, and E. Altman, A universal operator growth hypothesis, *Phys. Rev. X* **9**, 041017 (2019).
- [123] A. Dymarsky and M. Smolkin, Krylov complexity in conformal field theory, *Phys. Rev. D* **104** (2021) L081702.
- [124] A. Kundu, V. Malvimat, and R. Sinha, State dependence of Krylov complexity in 2d CFTs, *J. High Energy Phys.* **09** (2023) 011.
- [125] Z.-Y. Fan, Momentum-Krylov complexity correspondence, [arXiv:2411.04492](https://arxiv.org/abs/2411.04492).
- [126] A. Chattopadhyay, V. Malvimat, and A. Mitra, Krylov complexity of deformed conformal field theories, *J. High Energy Phys.* **08** (2024) 053.
- [127] D. Basu, Lavish, and B. Paul, Entanglement negativity in TT -deformed CFTs, *Phys. Rev. D* **107**, 126026 (2023).
- [128] D. Basu and V. Raj, Reflected entropy and timelike entanglement in TT -deformed CFTs, *Phys. Rev. D* **110**, 046009 (2024).